13th Serbian Conference on Spectral Line Shapes in Astrophysics

Radio-Loud Population A Quasars at High Redshift

Alice Deconto-Machado[1]
Ascensión del Olmo[1]
Paola Marziani[2]
Jaime Perea[1]
Giovanna Stirpe[3]
[1] IAA-CSIC, Spain; [2] INAF-Padova, Italy; [3] INAF-Bologna, Italy

Belgrade, August 26th 2021

OUTLINE

The Unified Model of Active Galactic Nuclei

An H-R Diagram for quasars?

What about the radioloudness?

Observations and Sample

Analysis

PKS2000-330

Q1410+036

Conclusions

THE UNIFIED MODEL OF ACTIVE GALACTIC NUCLEI

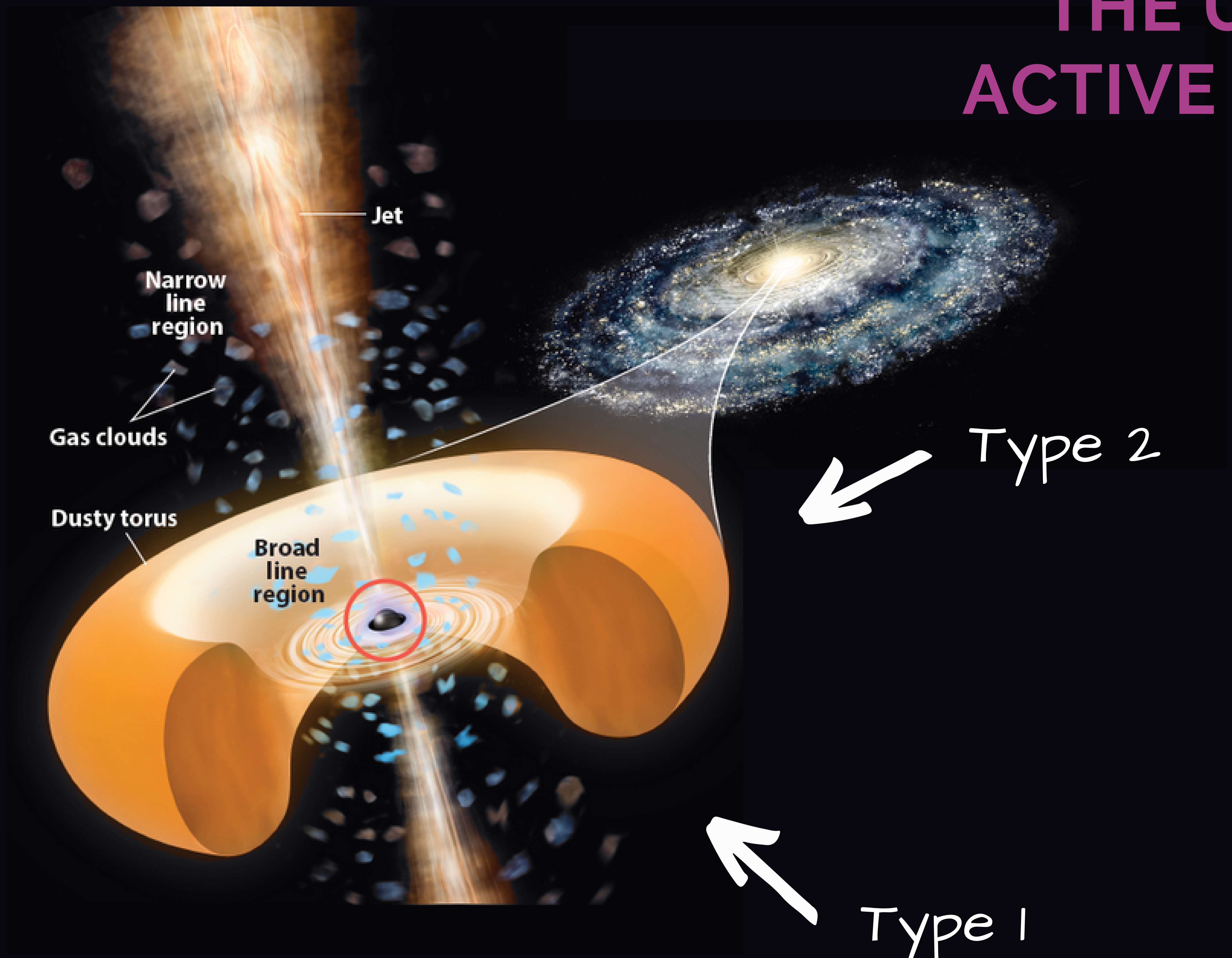

Type 2

Type 1

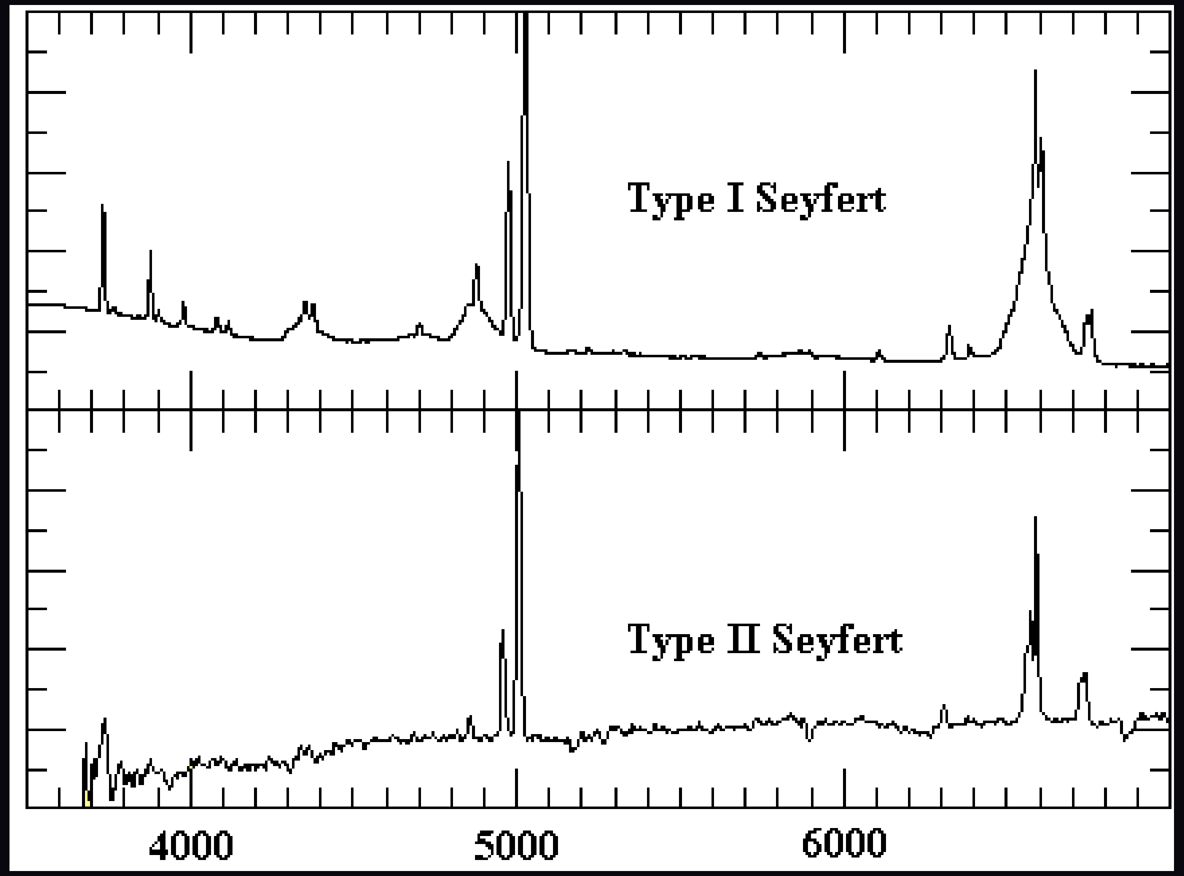

THE MAIN SEQUENCE

An H-R diagram for quasars?

(Sulentic, J. W.; Marziani, P.; Dultzin-Hacyan, D., 2000)

Zamfir et al., 2010

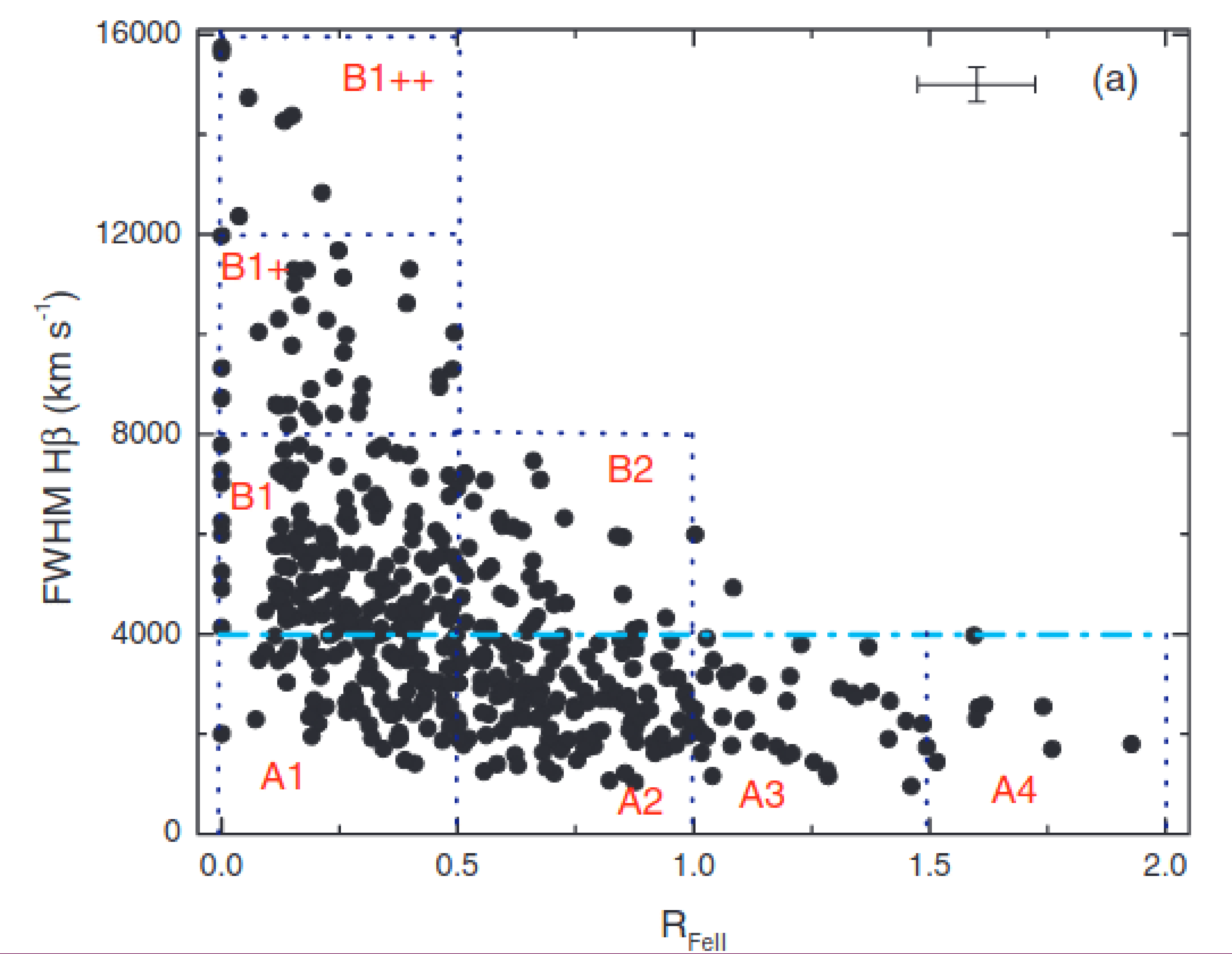

Optical plane of the **4DE1**

4DE1 MAIN PARAMETERS

- **FWHM(Hβ BC);**
- **RFeII = I(FeIIλ4570)/I(Hβ);**
- **BLUESHIFTS OF HIL;**
- **SOFT X-RAY PHOTON INDEX.**

Eddington ratio, λE = Lbol/LEdd, and **orientation** are thought to be the main physical drivers of the MS.

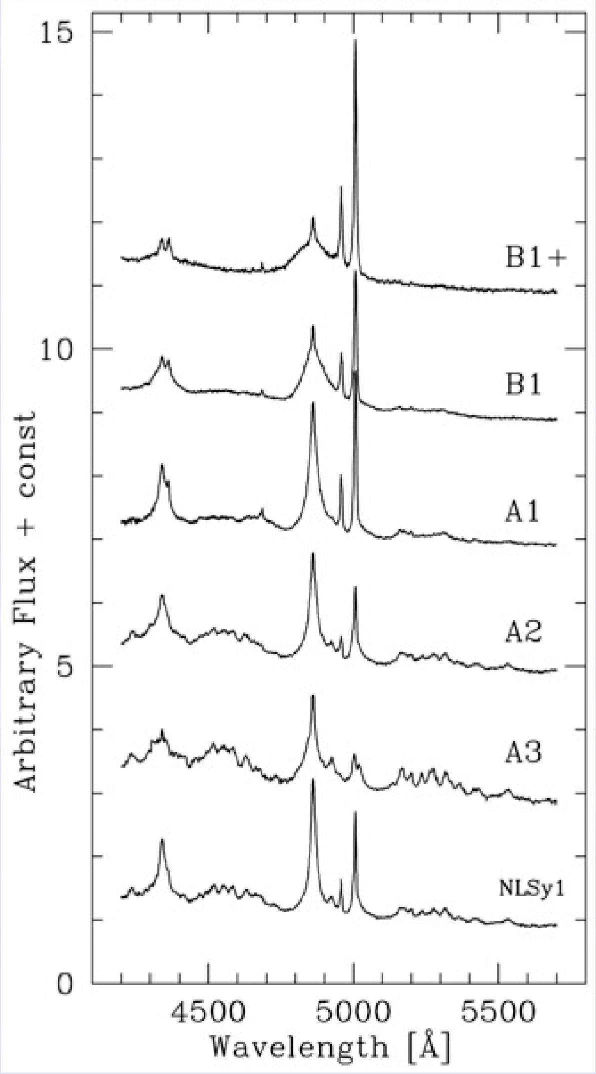

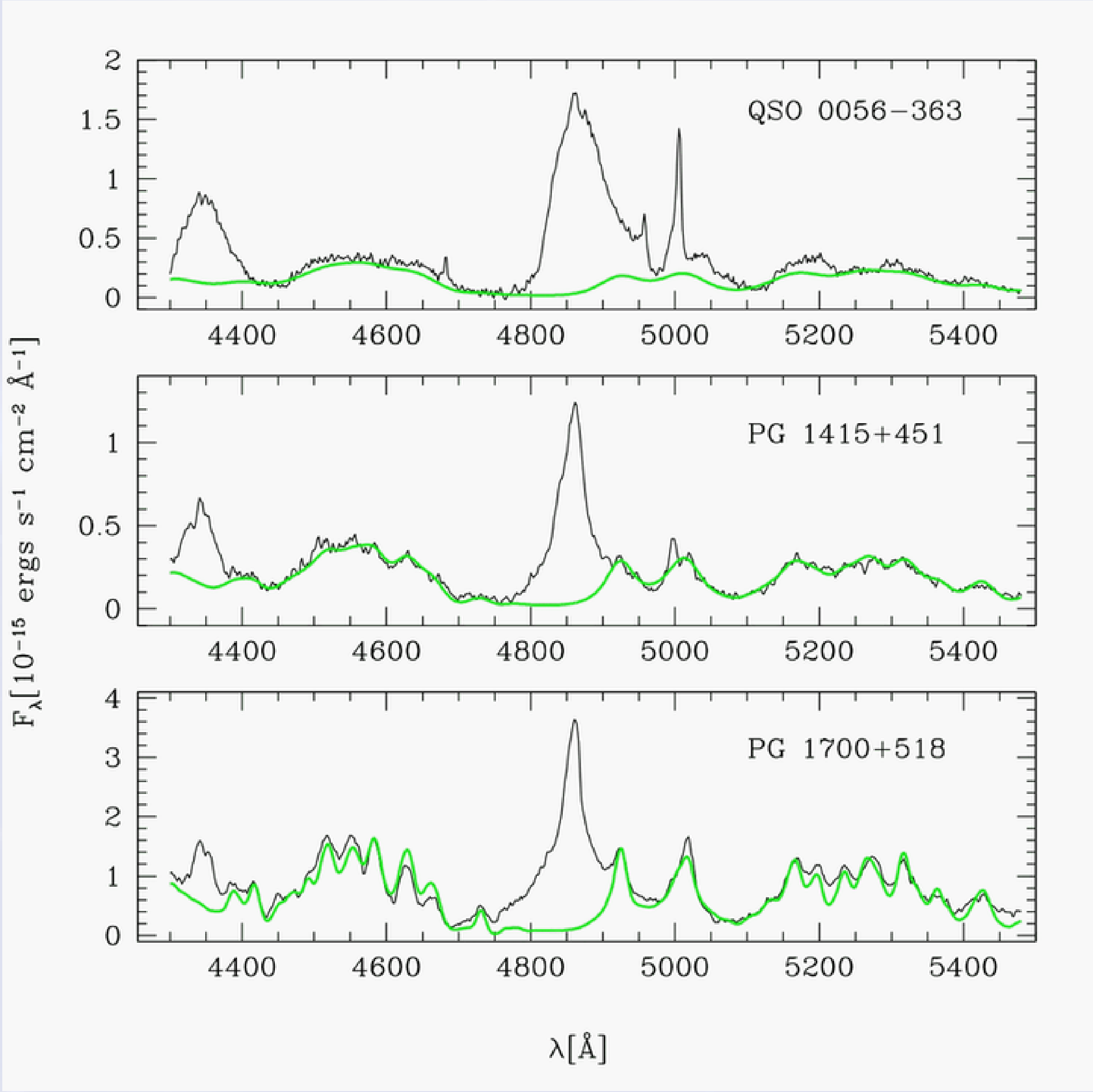

Marziani et al., 2018

POP. A VS. POP. B

Population A: FWHM(Hβ) ≤ 4000 km/s, and with ST defined by increasing RFeII from A1 with RFeII < 0.5 to A4 with 1.5 ≤ RFeII ≤ 2;

Population B: FWHM(Hβ) > 4000 km/s, and ST bins defined in terms of increasing ΔFWHM(Hβ) = 4000 km/s.

Pop. B quasars are the ones with **high MBH** and **low λE**, while **Pop. A** are **fast-accreting** with relatively **small MBH**.

Panda et al., 2019

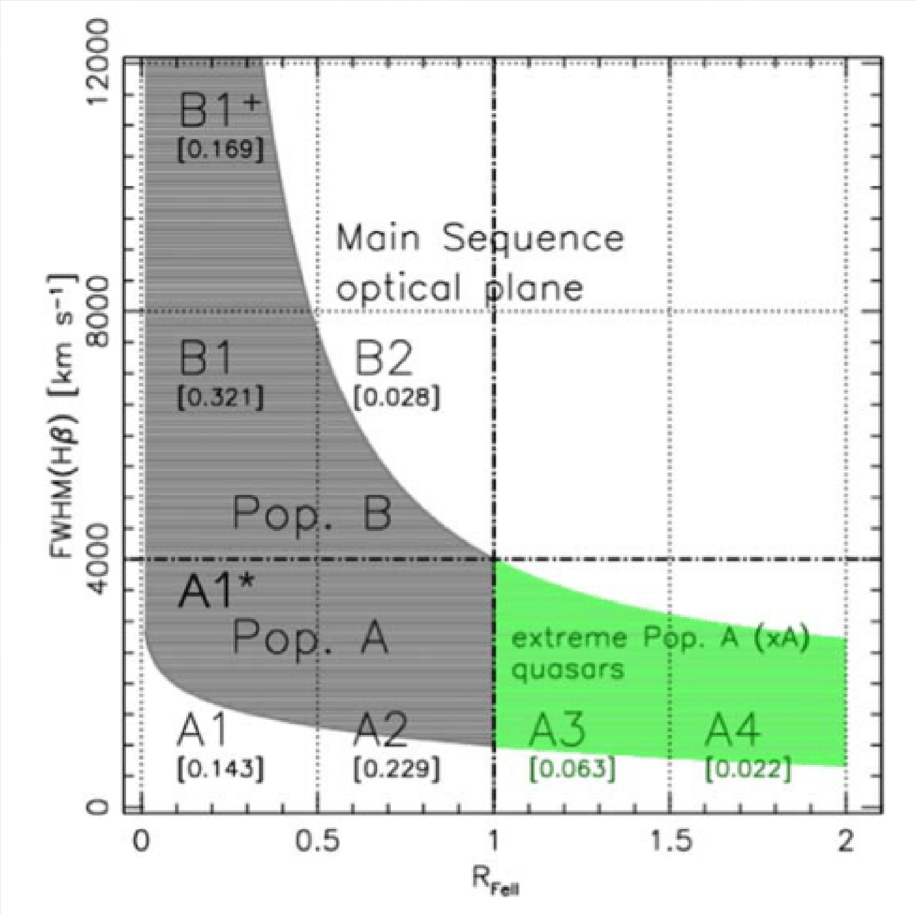

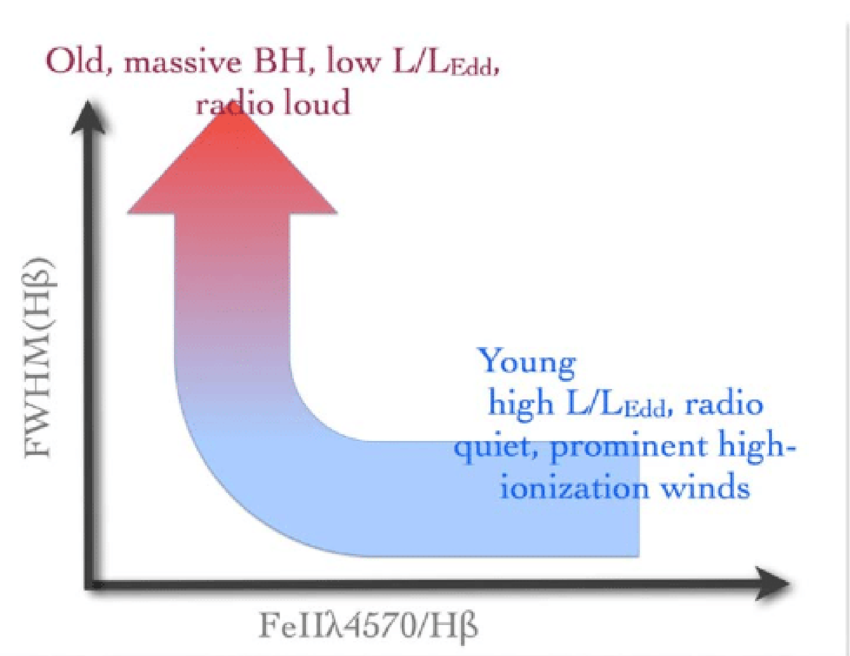

Hβ profile evolution through different luminosity ranges

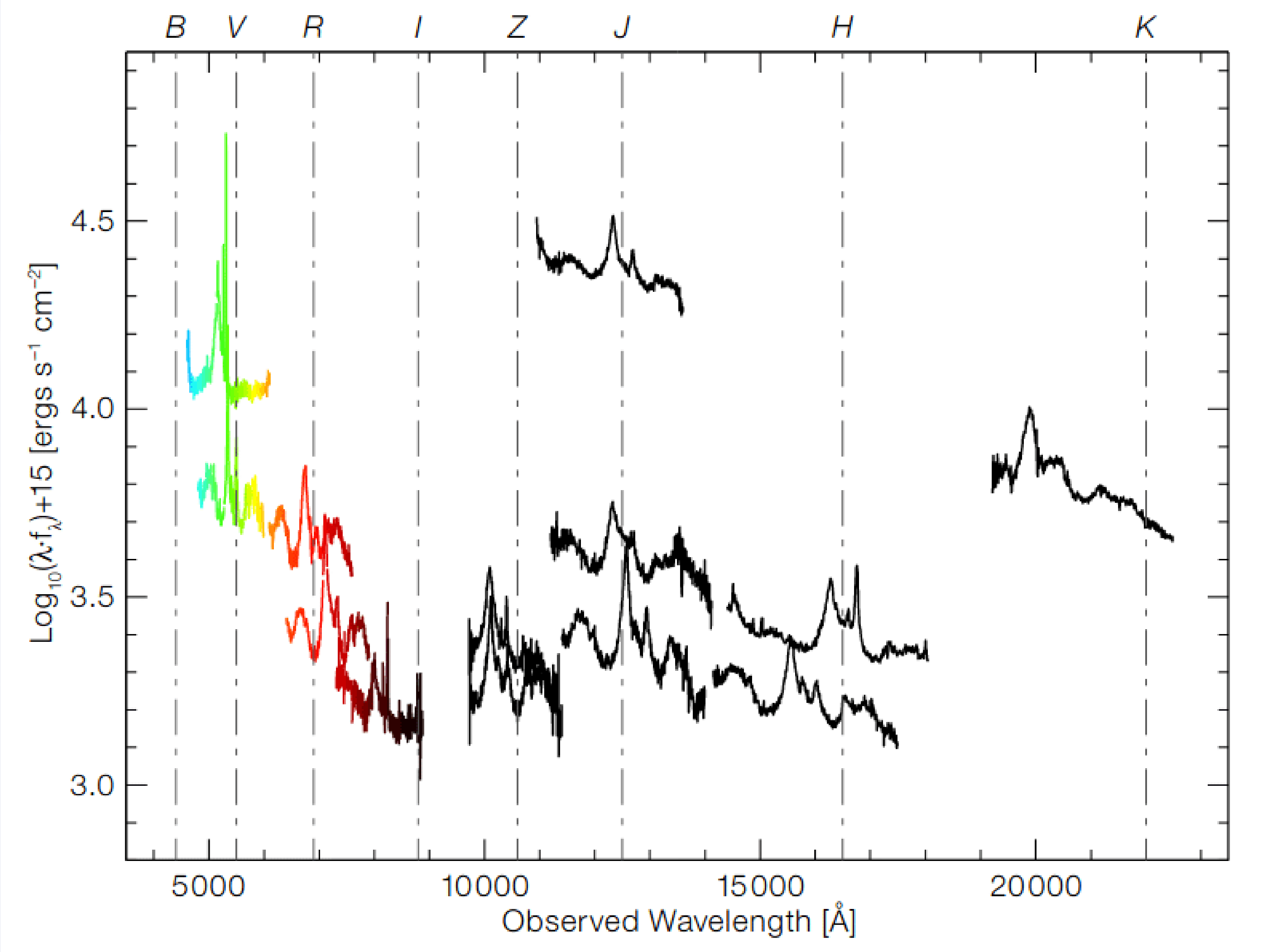

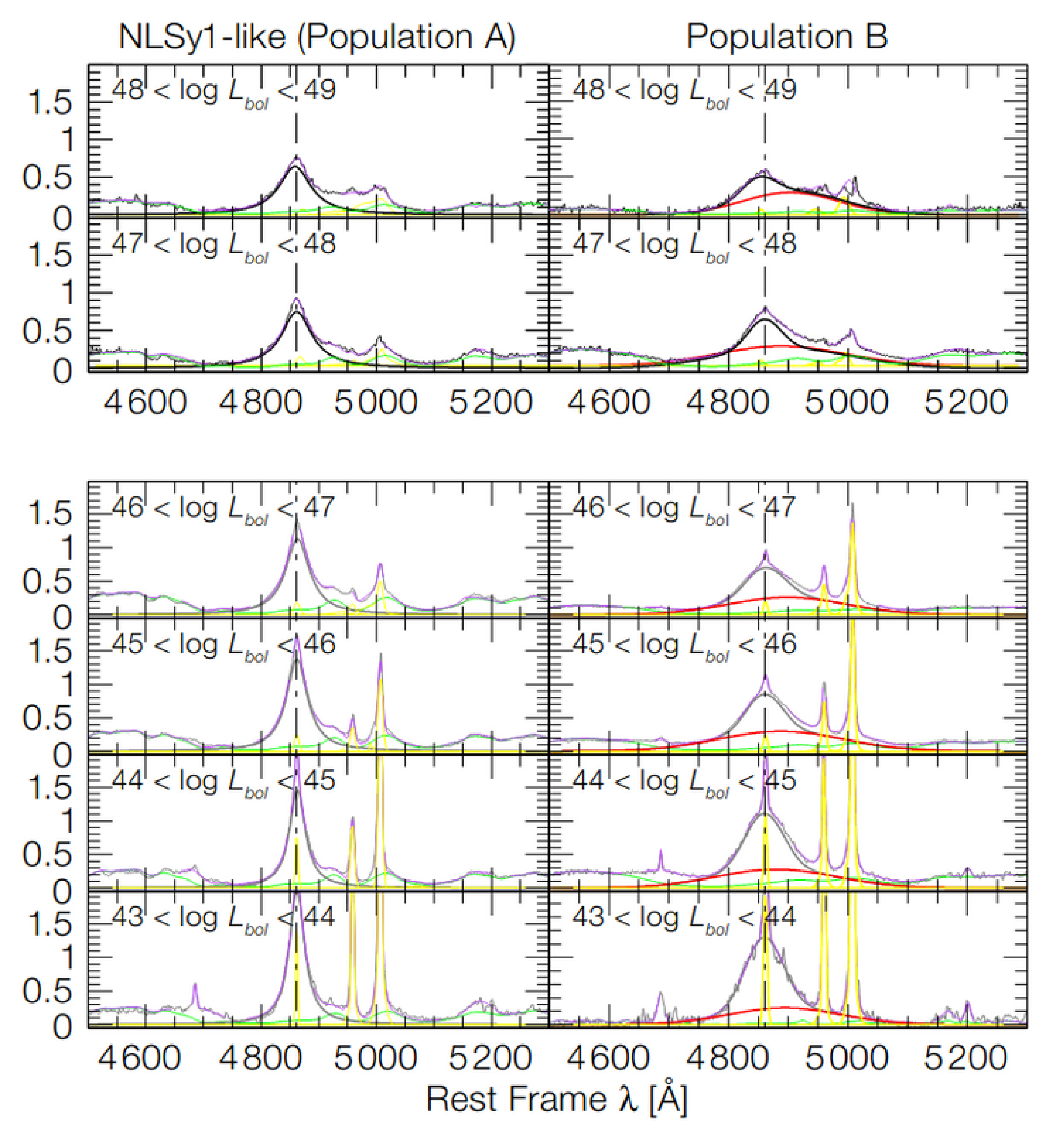

Sulentic et al., 2009

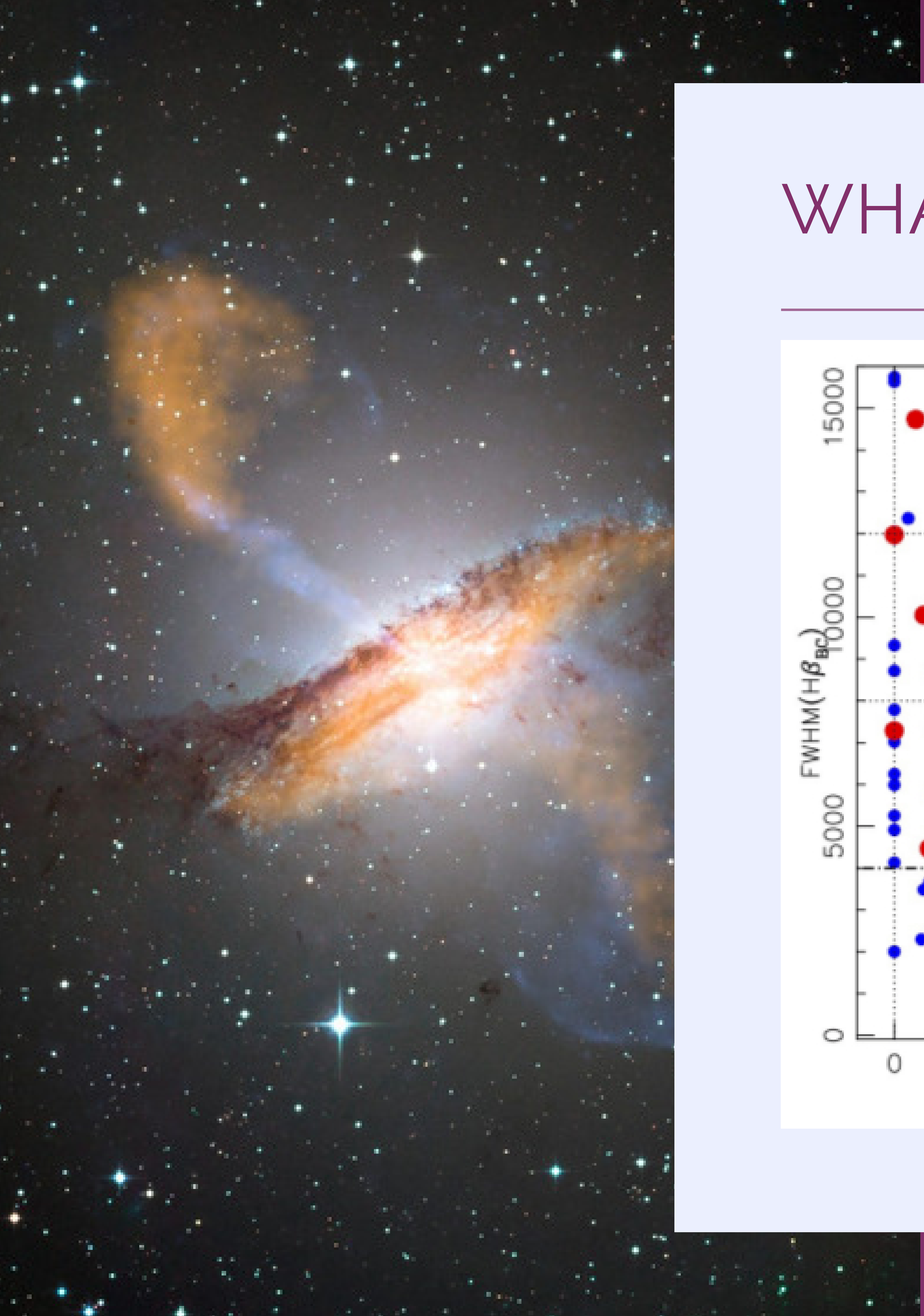

WHAT ABOUT THE **RADIOLOUDNESS?**

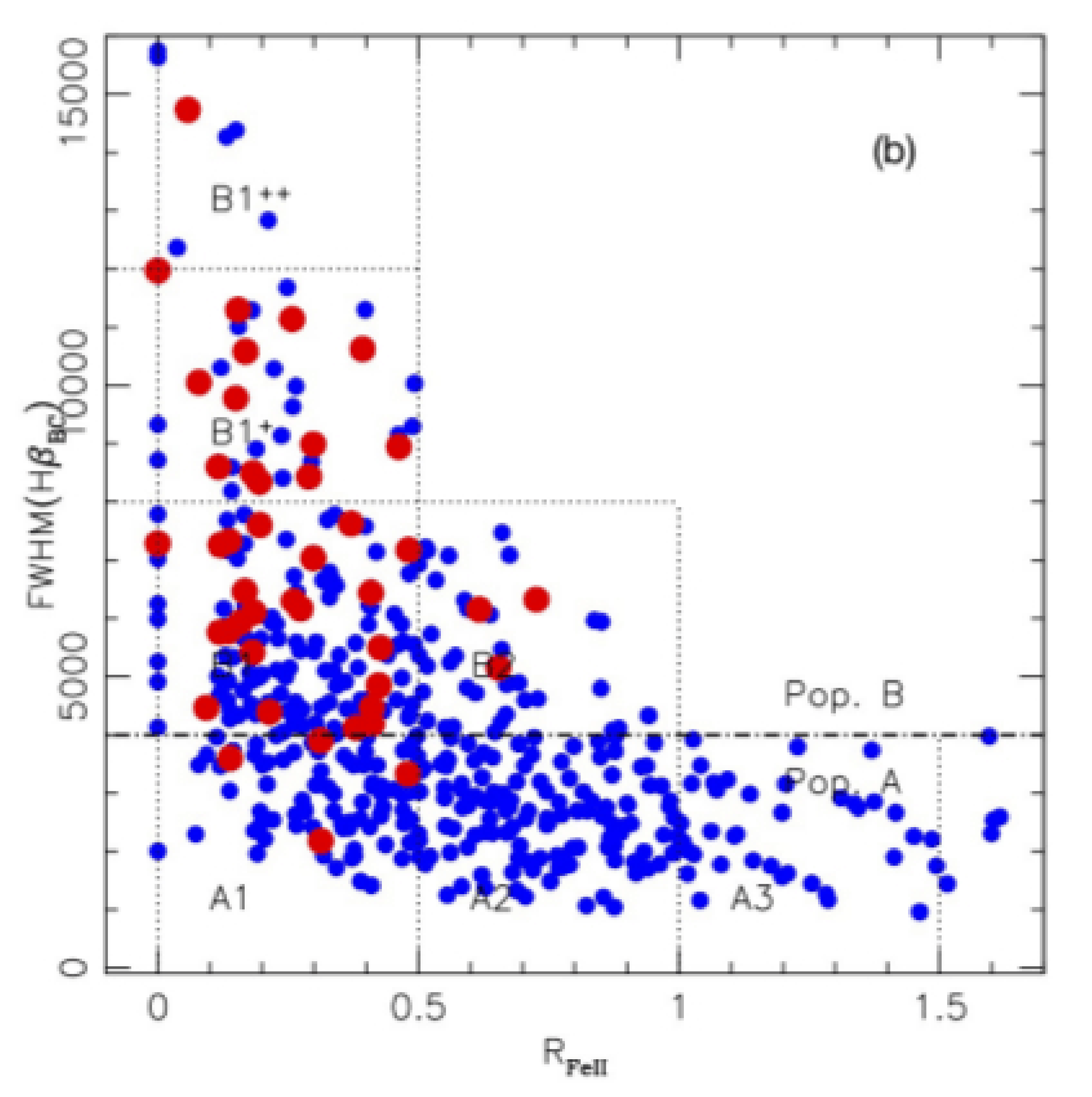

Zamfir et al., 2010

$$R_L = f_{radio}/f_{optical}$$

RL (jetted) quasars **are not distributed uniformly along the MS**. They are predominantly found in the Pop. B domain.

OBSERVATIONS

VLT

OBSERVATIONS

- ISAAC spectrograph at the VLT (slit width of 0.6'');

- Data archive from NVSS, FIRST, GTC, WISE, GALEX, PanStar, and others;

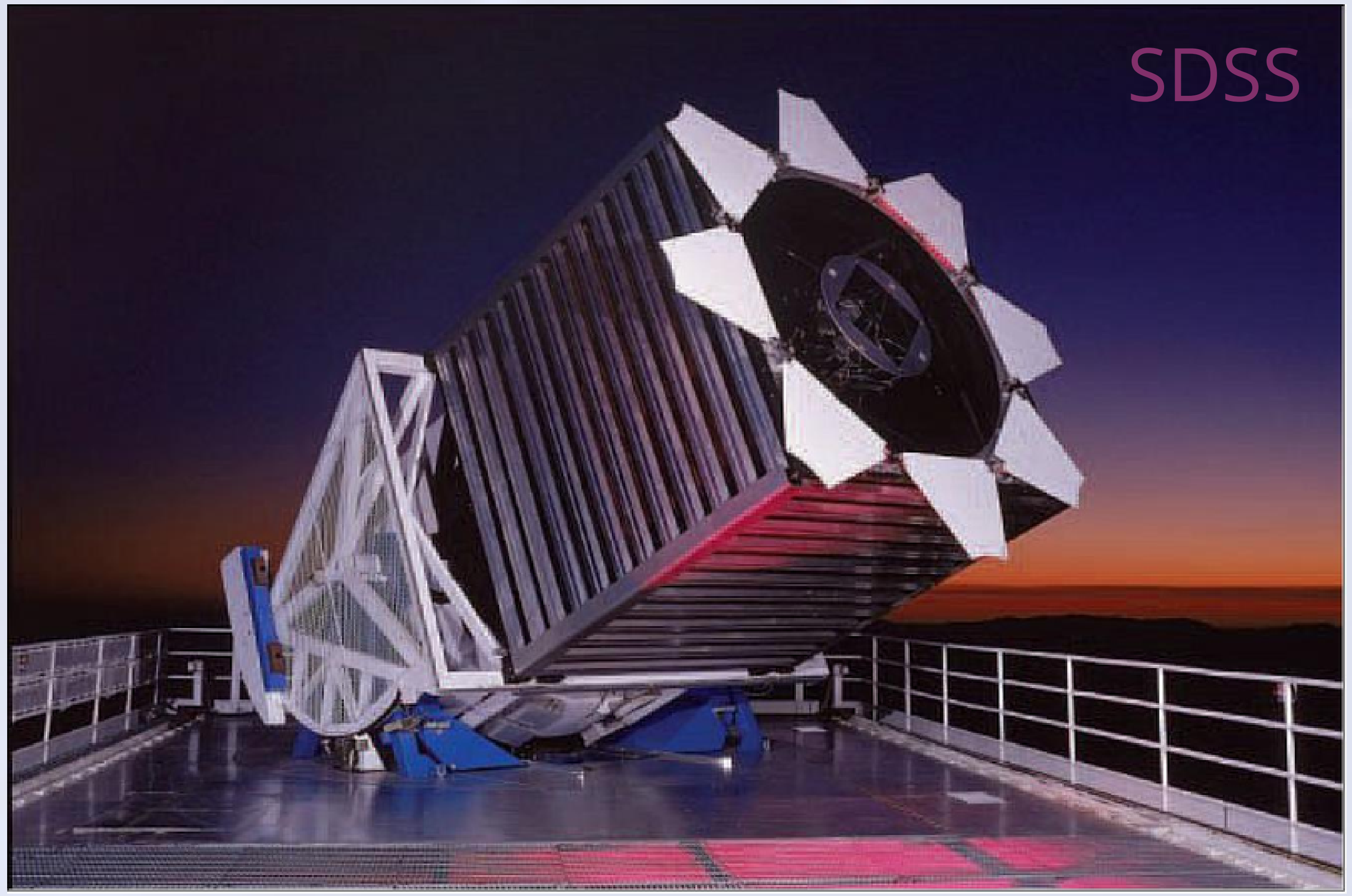

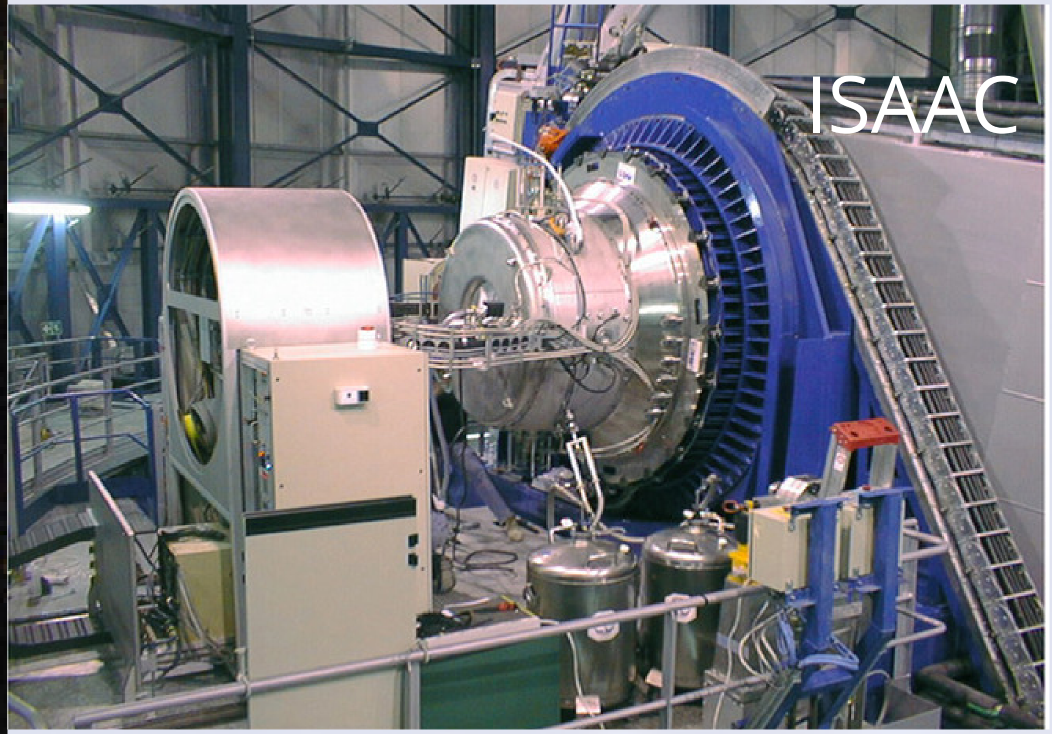

SAMPLE

SAMPLE: High luminosity QSOs with z = 1.4 - 3.8, including radio-loud and radio-quiet sources.

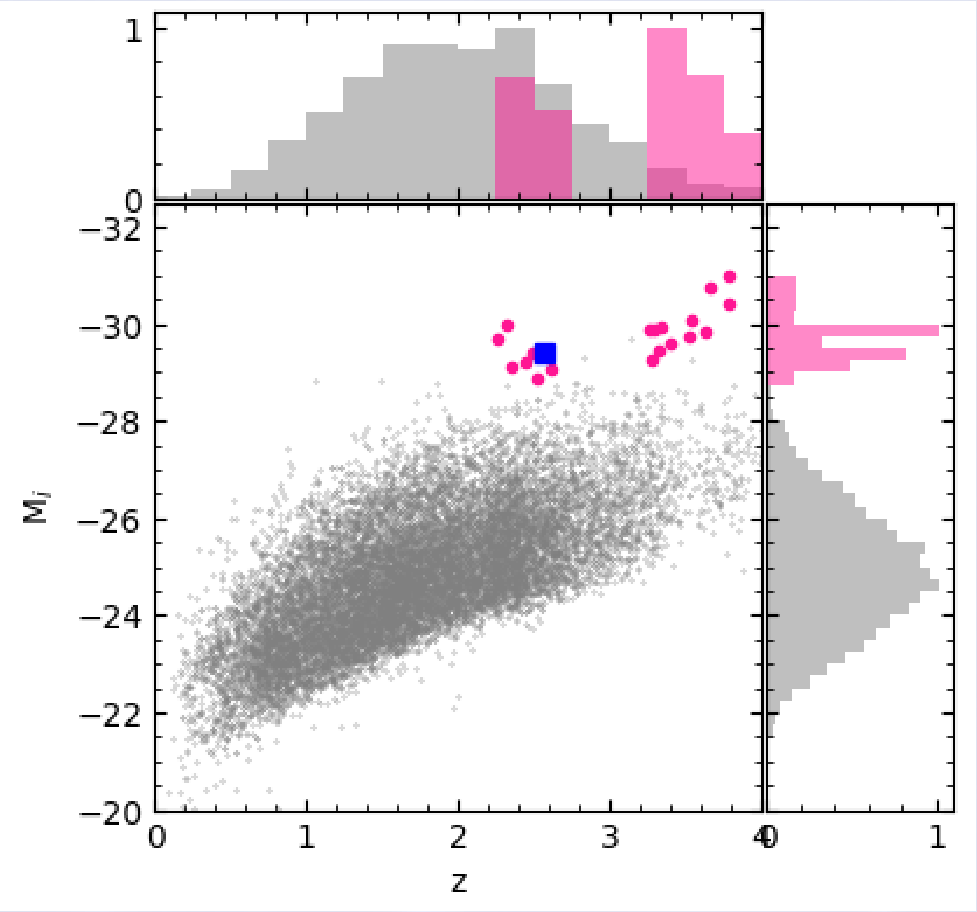

Optical:

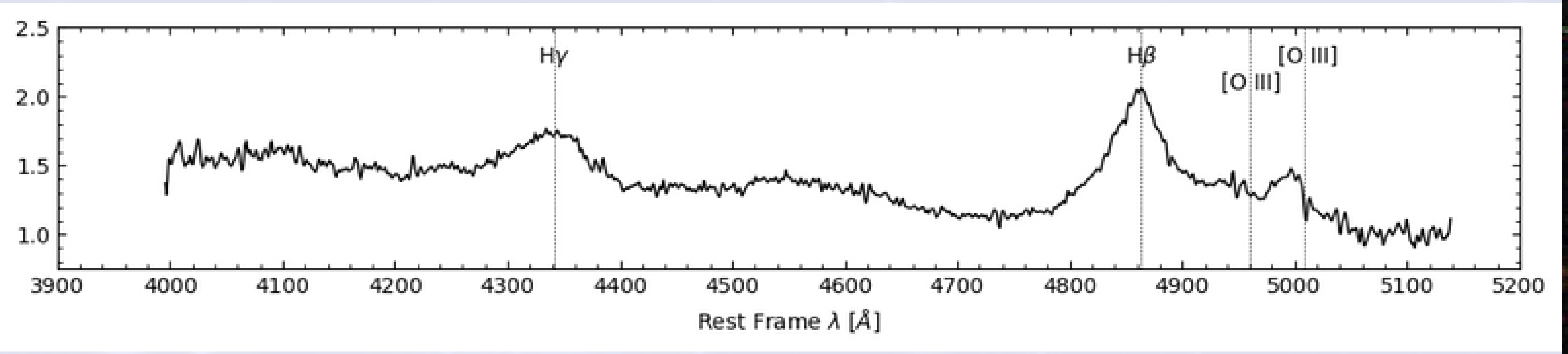

UV:

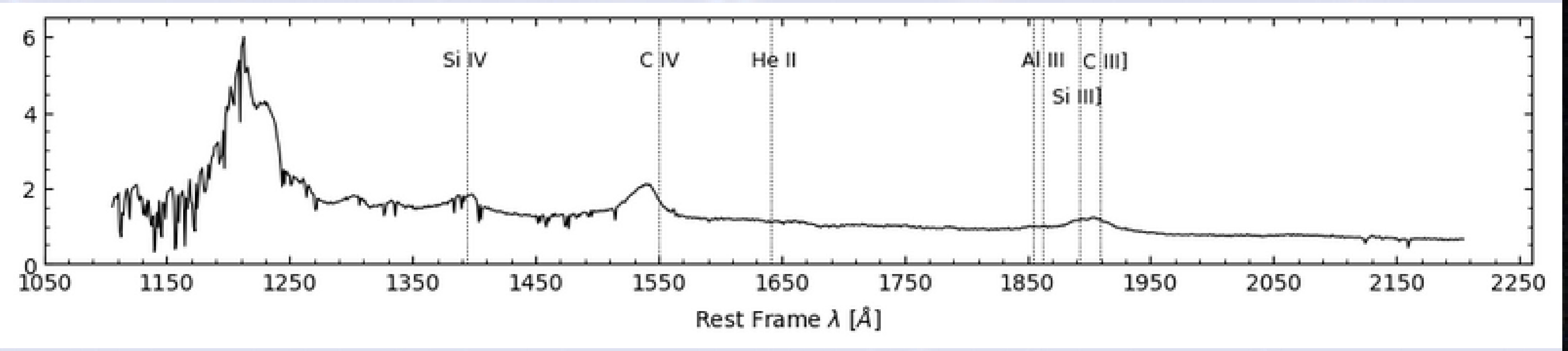

SAMPLE DISTRIBUTION IN THE MS

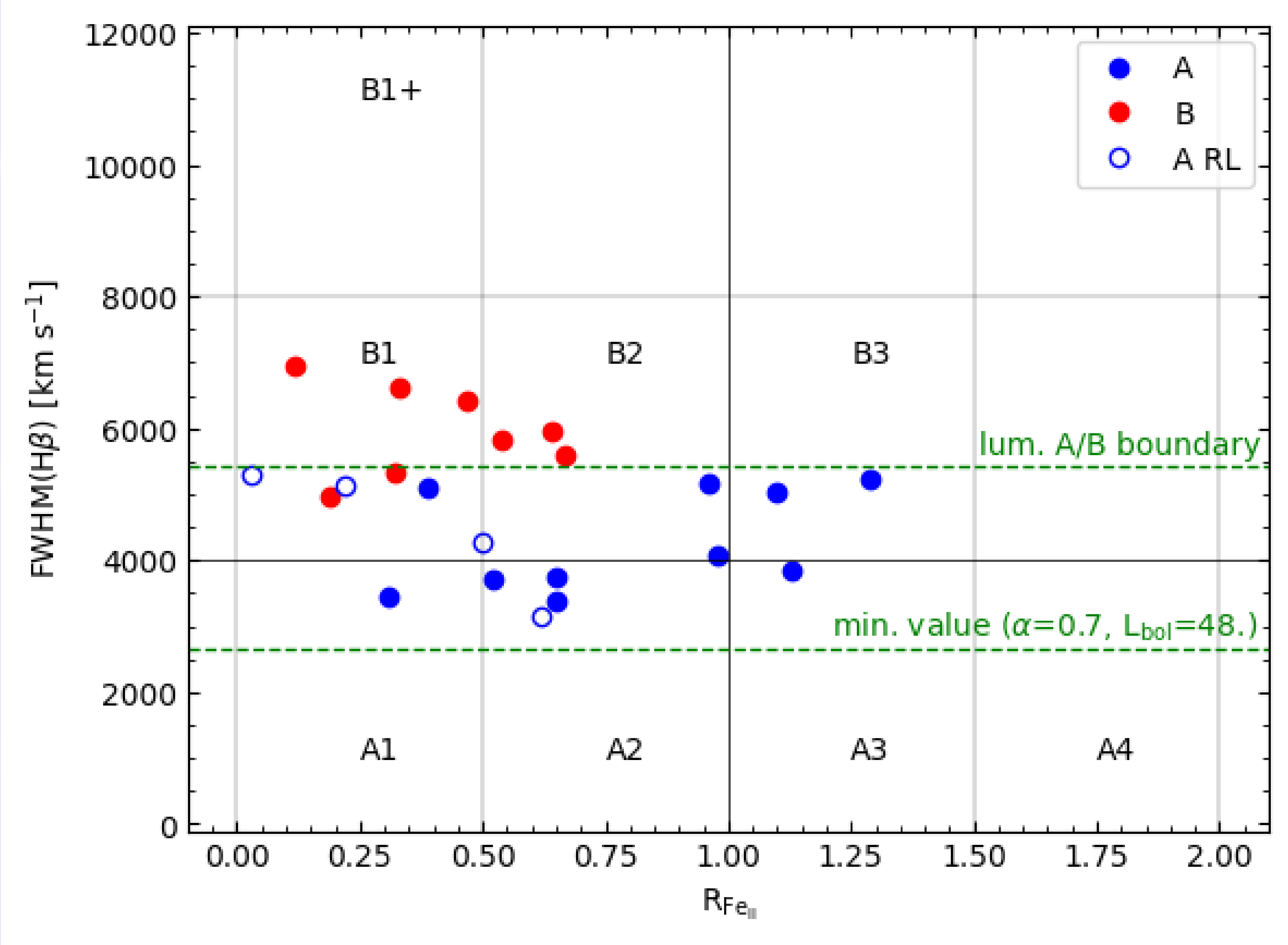

Marziani et al., 2021 (subm.)

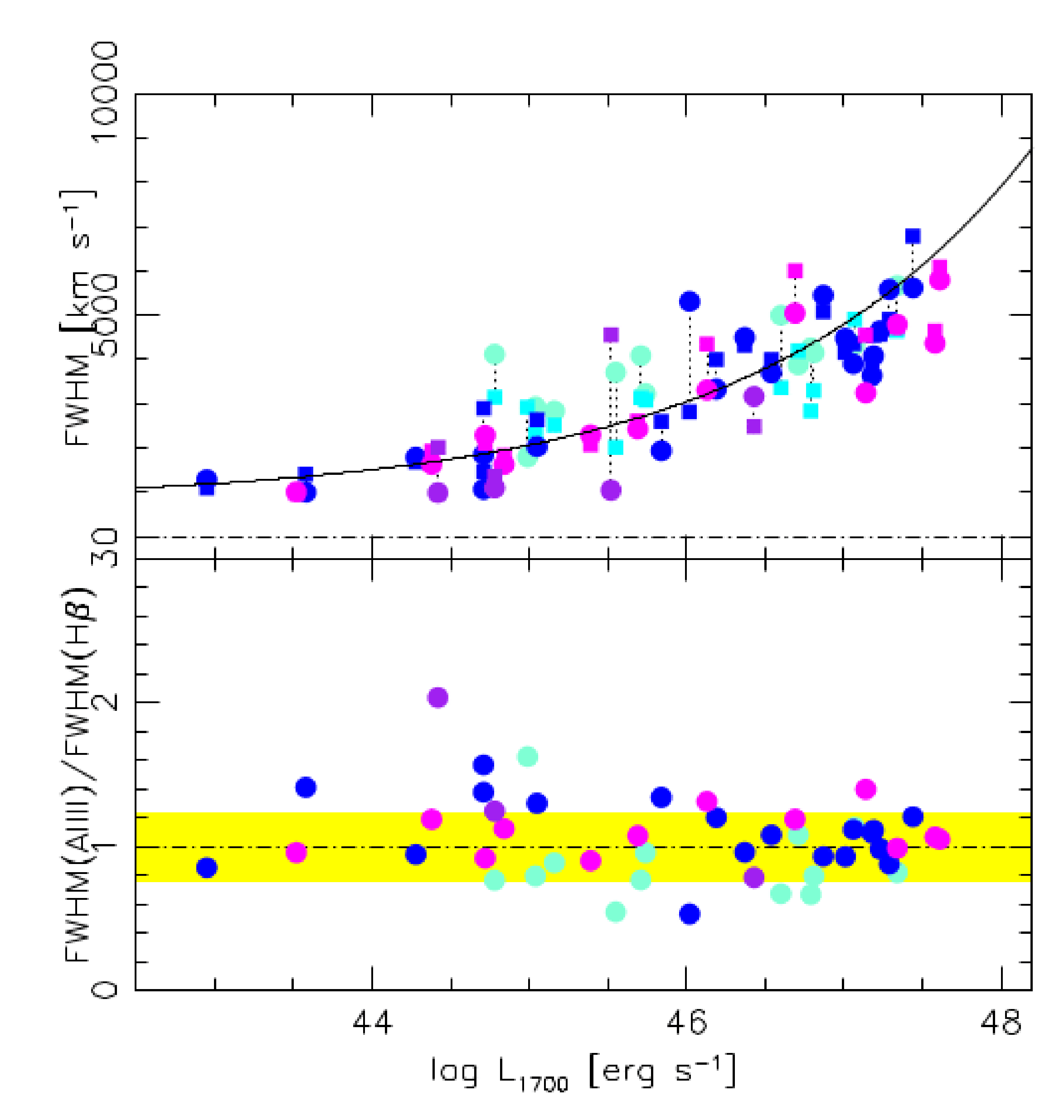

SAMPLE DISTRIBUTION IN THE MS

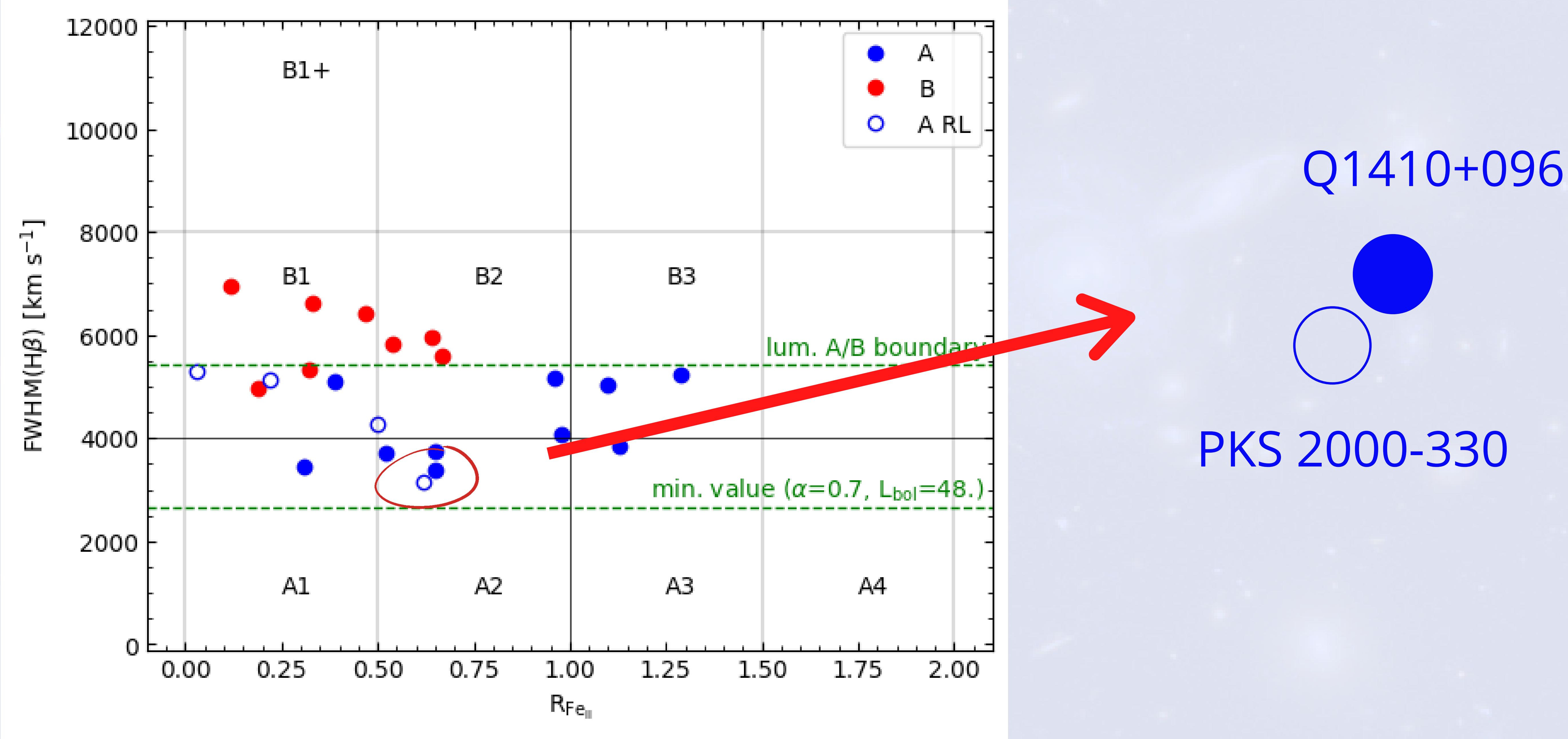

SAMPLE DISTRIBUTION IN THE MS

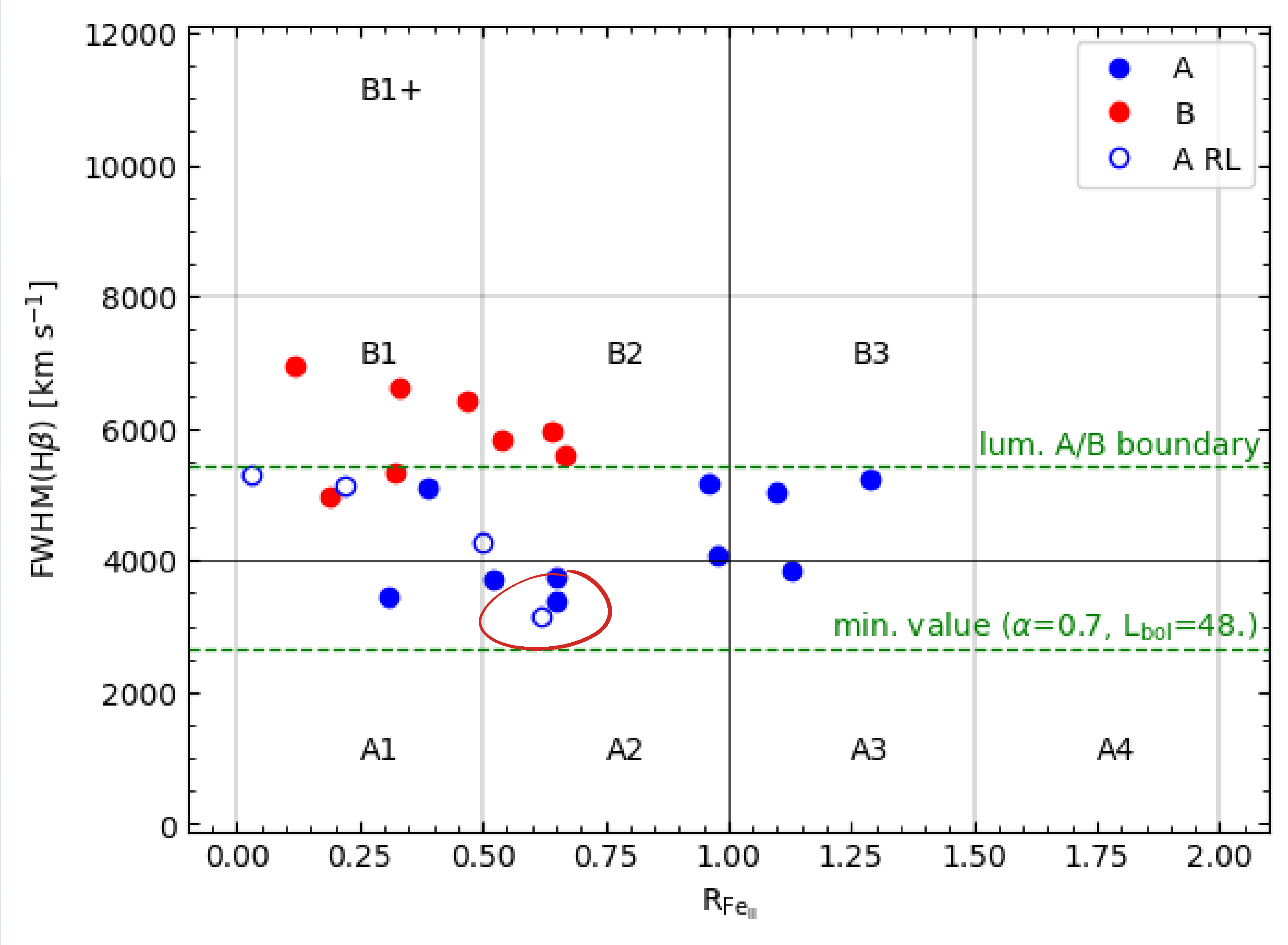

PKS 2000-330

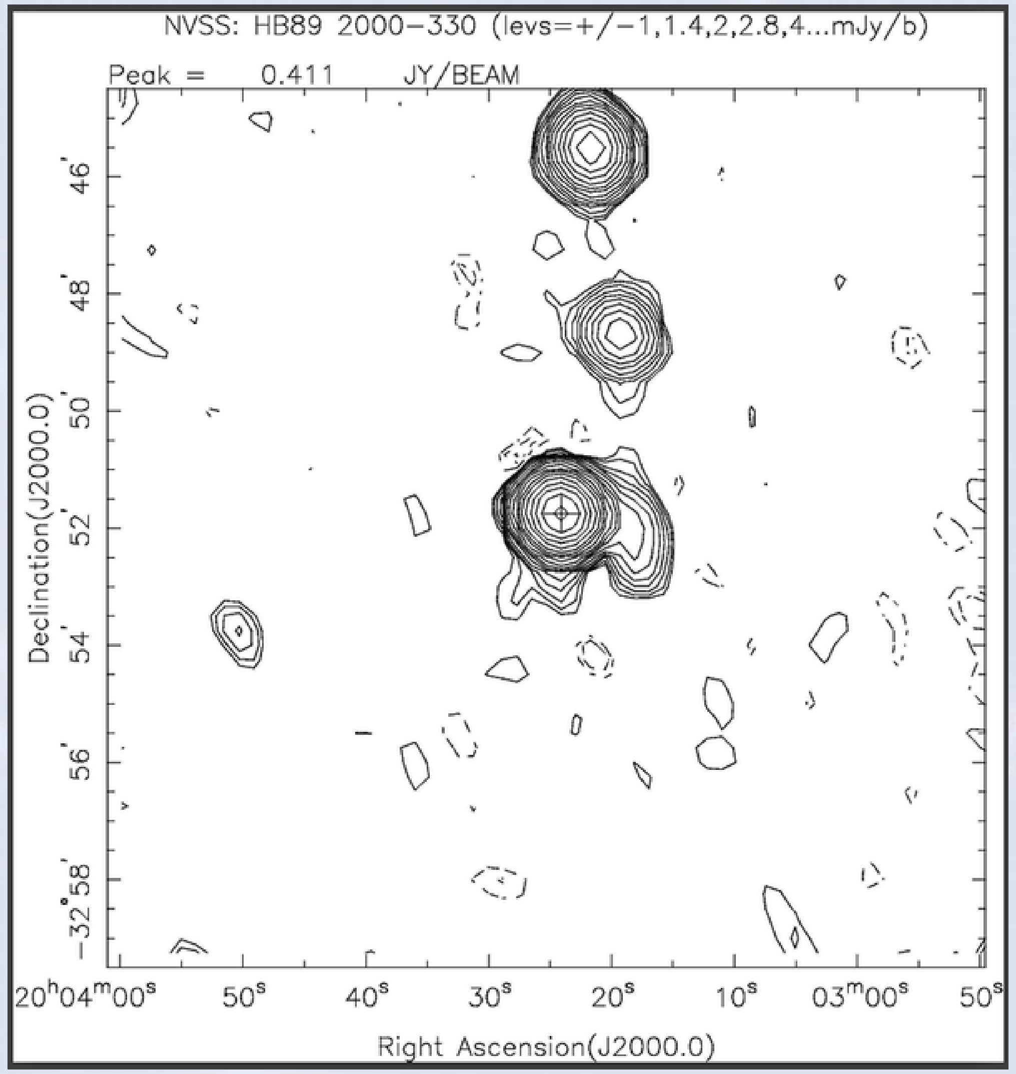

NVSS radio flux: 446.0±15.7 mJy

Radioloudness parameter: 4118.05

PKS 2000-330

- Radio-Loud
- z = 3.789
- FWHM (Hβ) = 3138±276 km/s
- RFe = 0.62
- Pop. A2

Q1410+096

- Radio-Quiet
- z = 3.3240
- FWHM (Hβ) = 3394±299 km/s
- RFe = 0.65
- Pop. A2

ANALYSIS

Multicomponent Fitting of the optical region (Hβ+[O III]λλ4959,5007)

Non-linear multicomponent fitting including the continuum (a power law), a semi-empirical scalable Fe II emission template and the emission line components

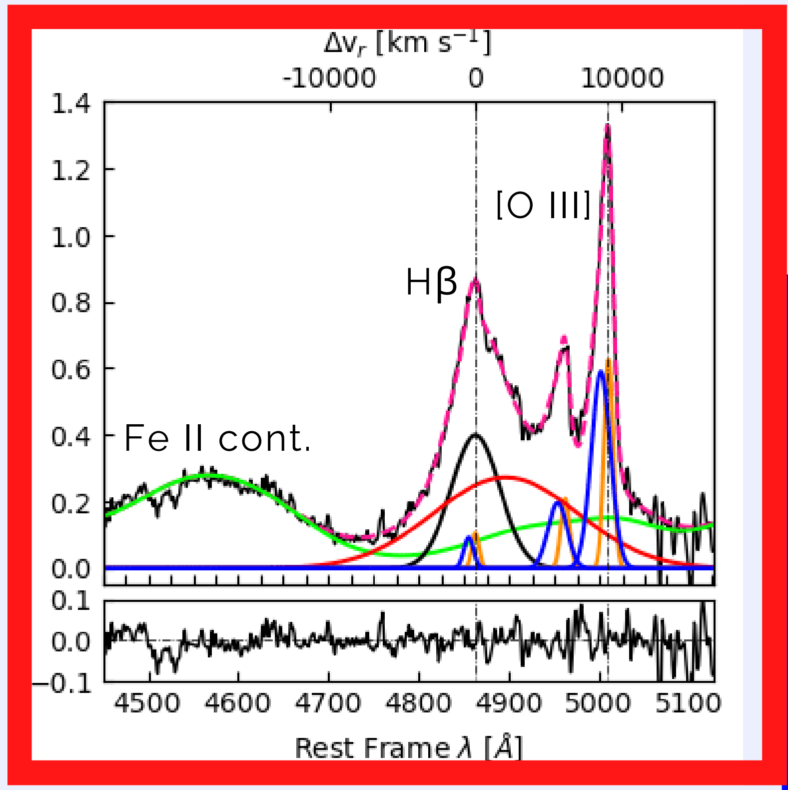

Pop. B

Pop. A

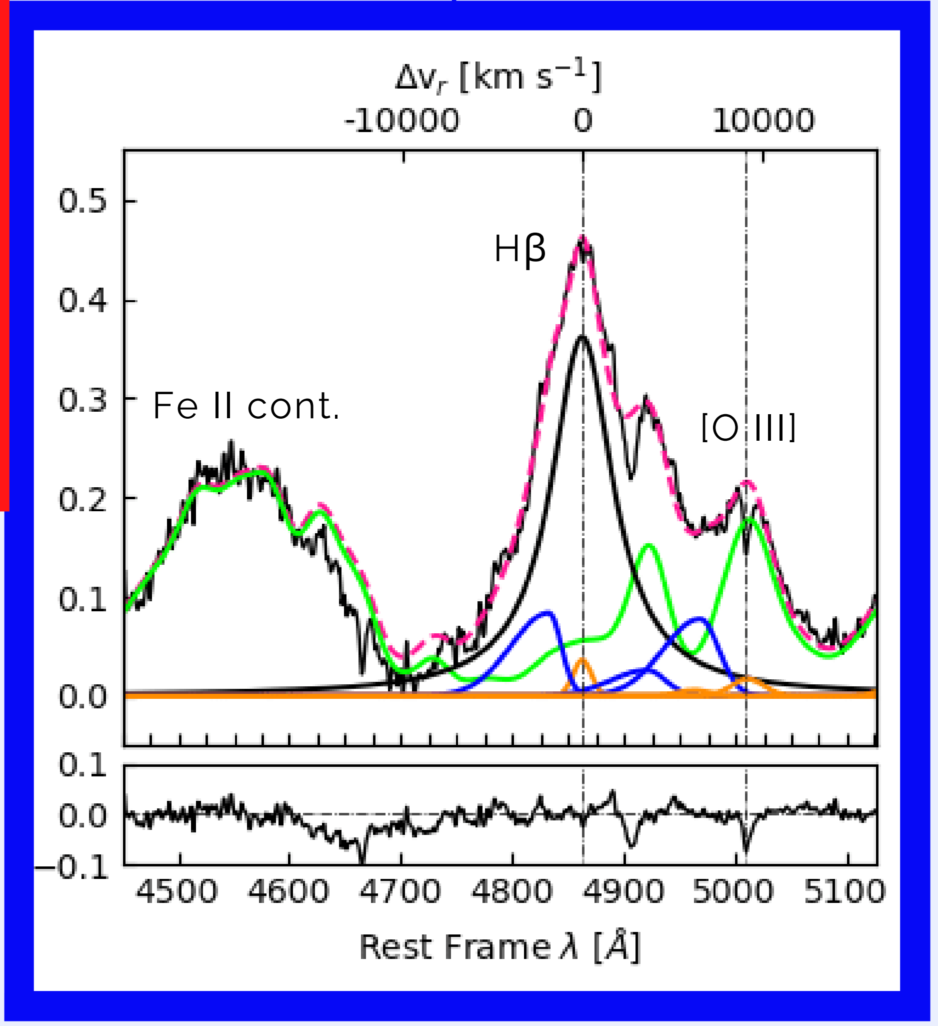

Broad Profile of Hβ:

- **BC:** Broad component symmetric and unshifted profile (Lorentzian for Pop. A or Gaussian for Pop. B);
- **BLUE:** Blueshifted component, present mainly in Pop. A quasars;
- **VBC:** Very broad Gaussian redshifted component clearly observed in Pop. B quasars;
- **NC:** Narrower component superimposed to the broad emission line profile.

ANALYSIS

Multicomponent Fitting of the UV region

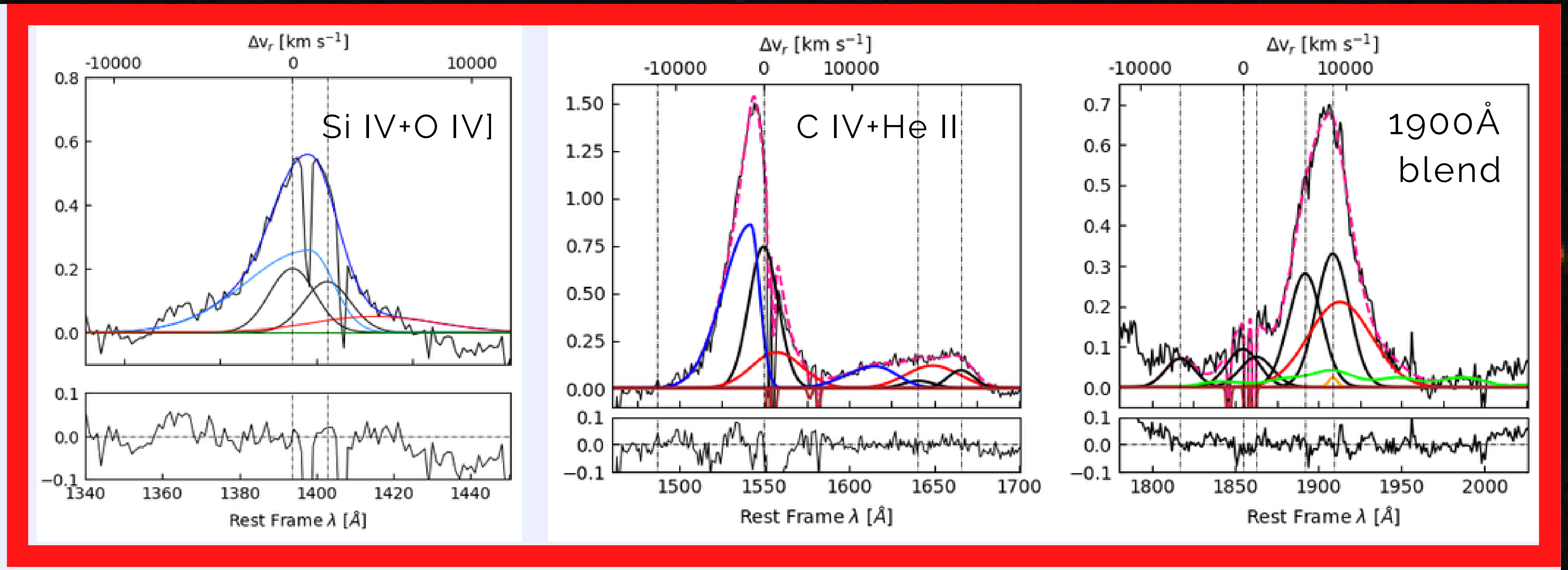

Following similar procedures as done for Hβ for the regions:

- 1900Å blend (Al III]λ1857 doublet, Si III]λ1892, and C III]λ1908);
- C IVλ1549+He IIλ1640;
- Si IVλ1397+O IV]λ1402.

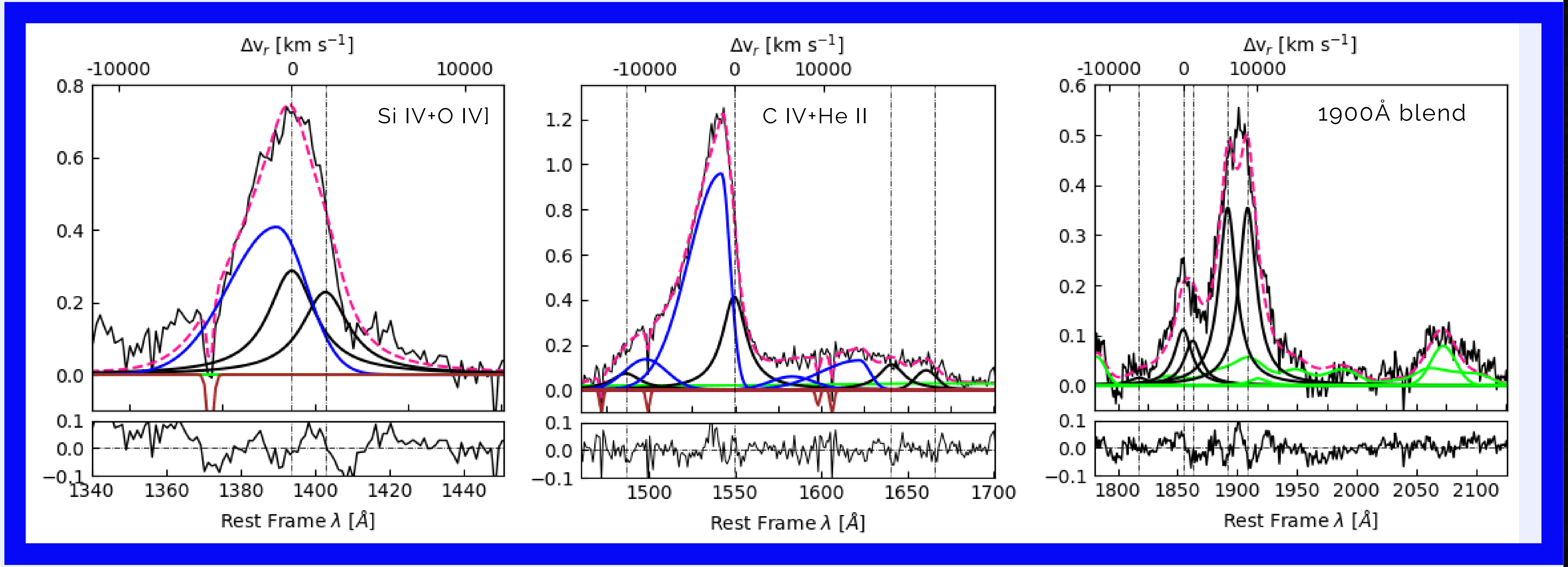

PKS 2000-330

Optical

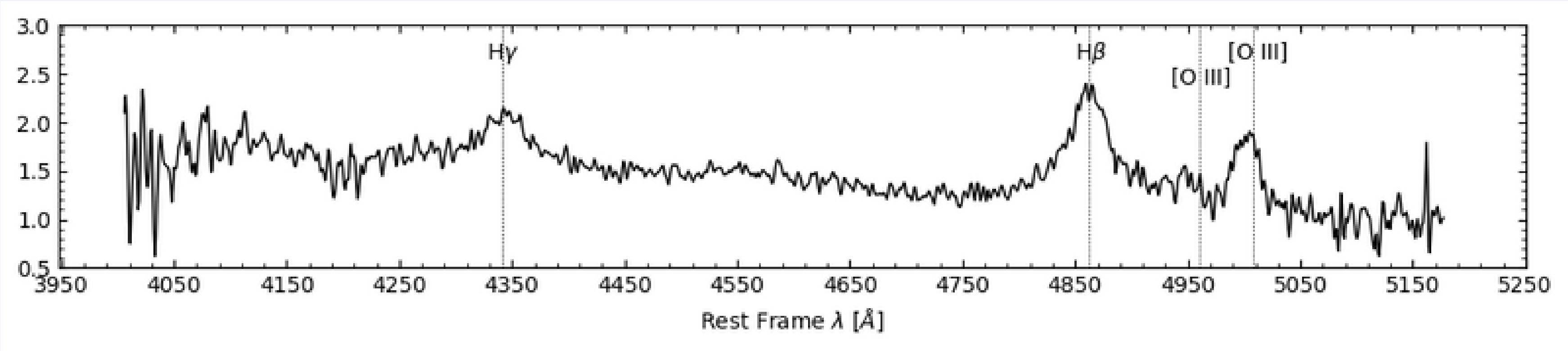

UV

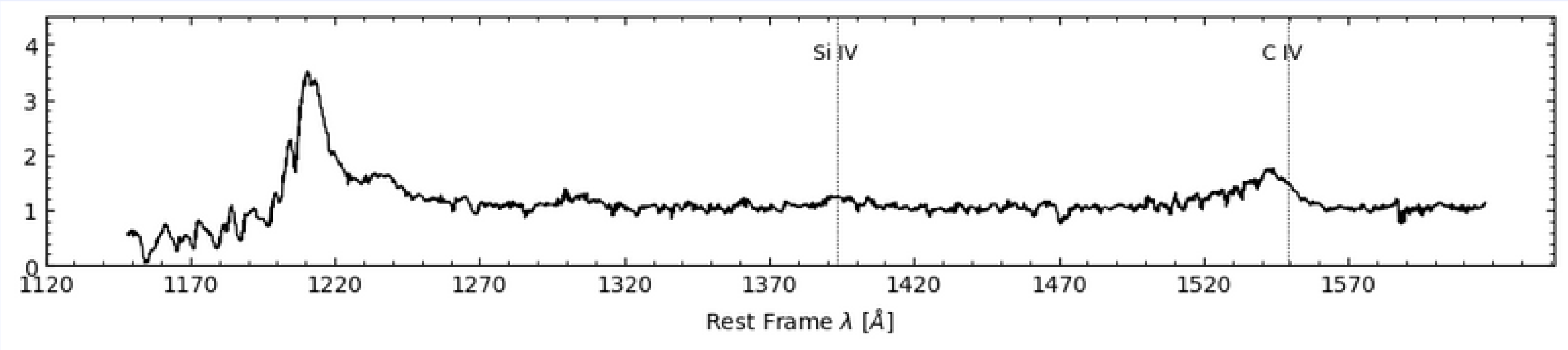

Barthel et al., 1990

Q1410+096

Optical

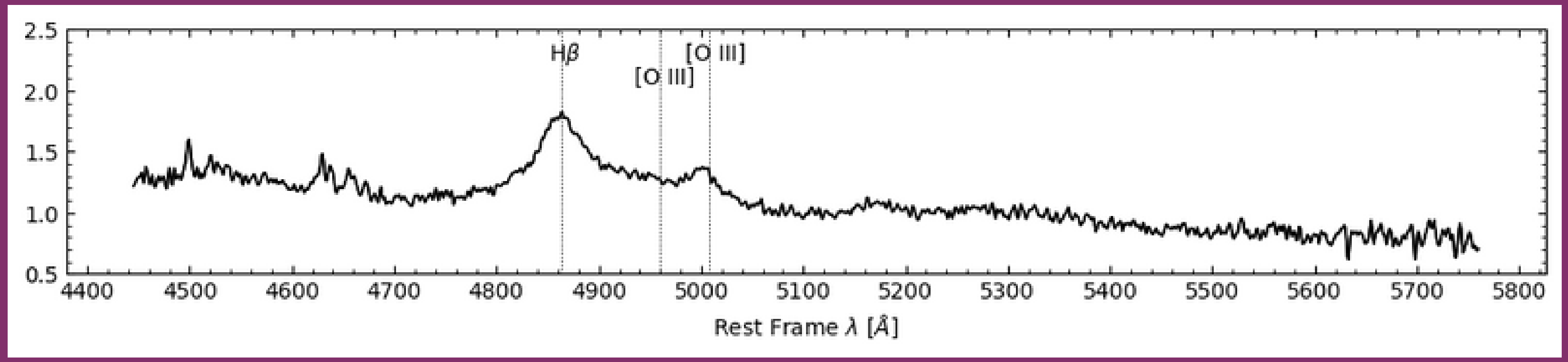

UV

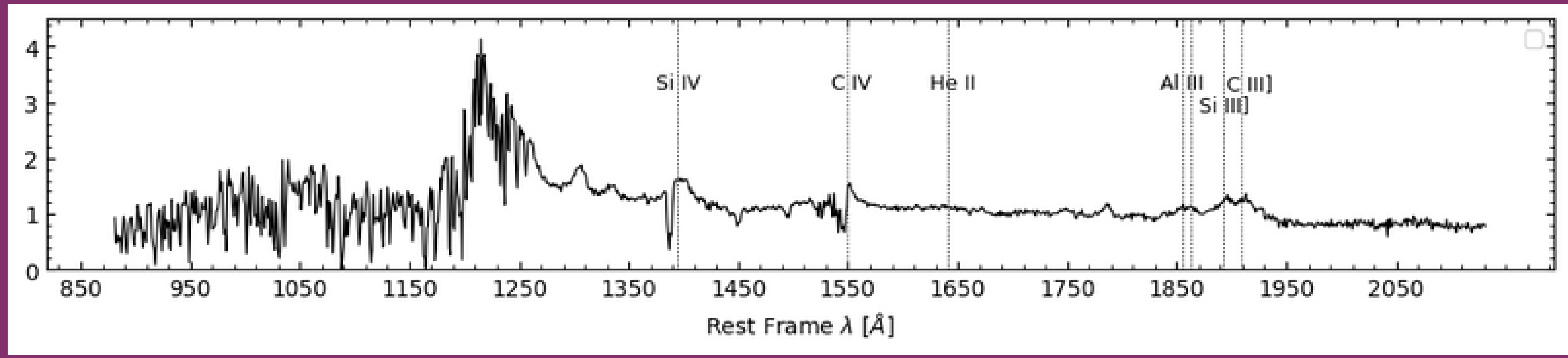

ANALYSIS - **PKS2000-330** & **Q1410+096**

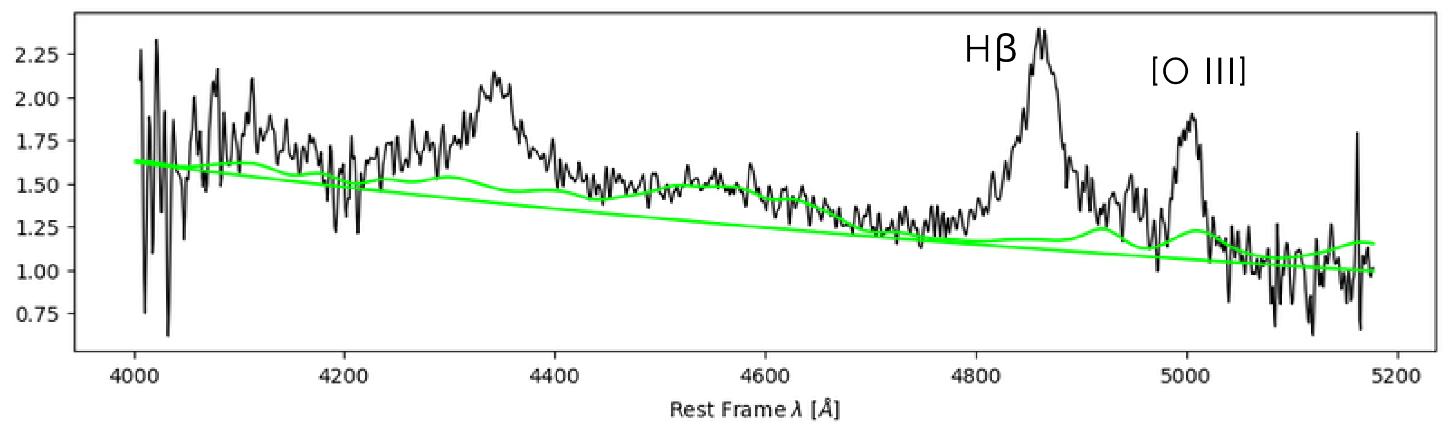

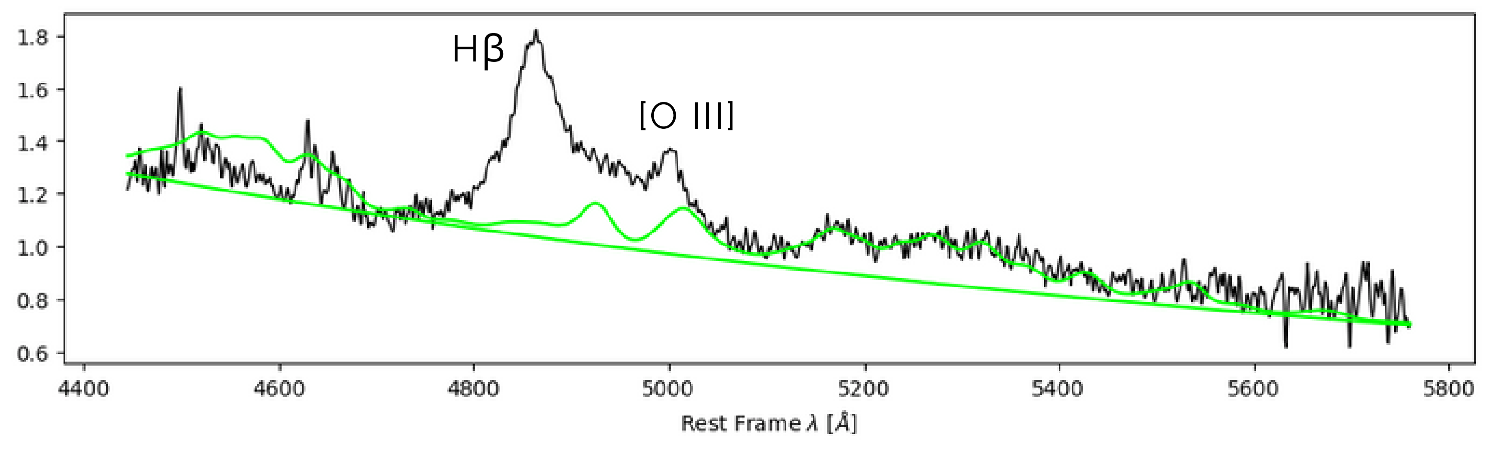

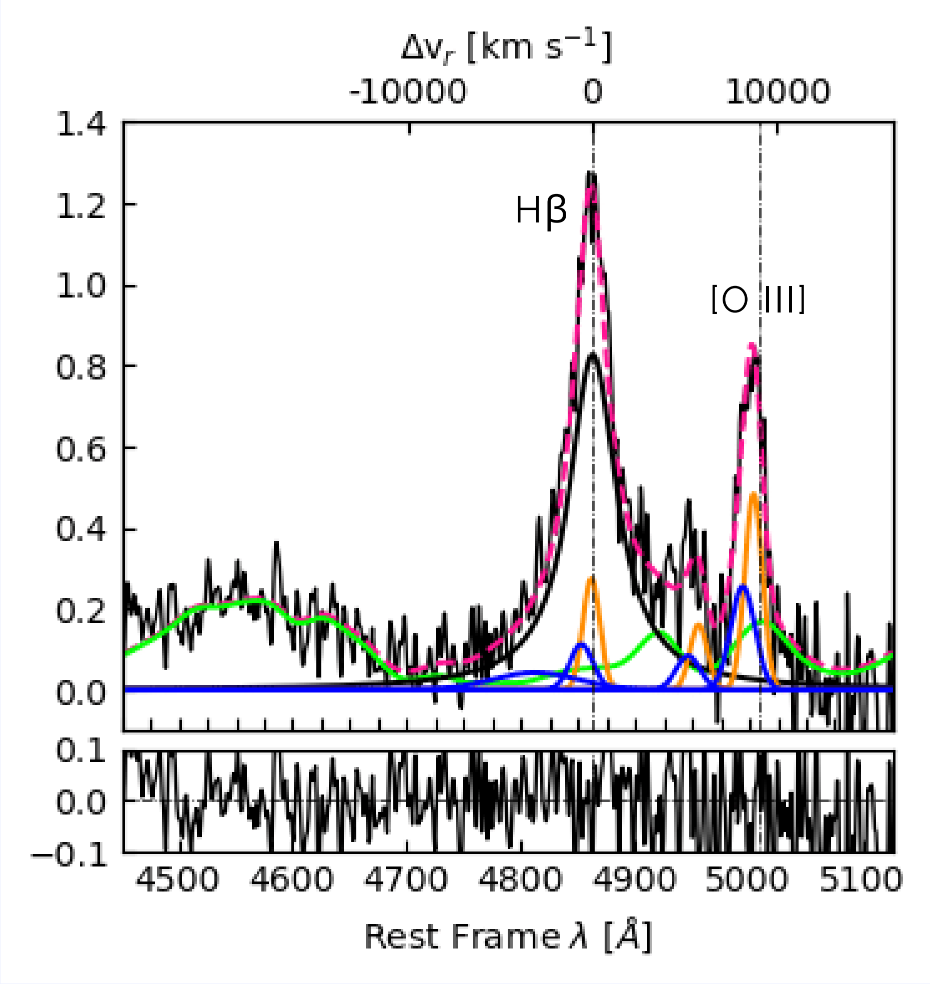

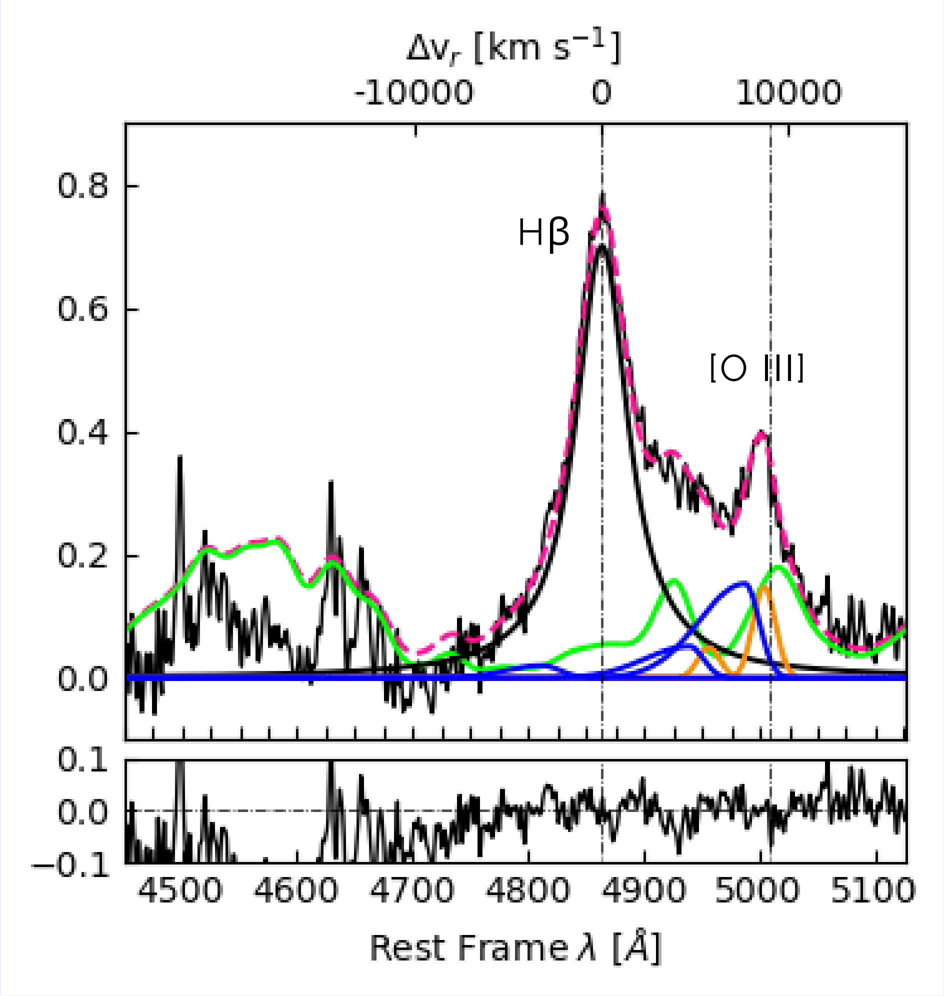

ANALYSIS - **PKS2000-330** & **Q1410+096**

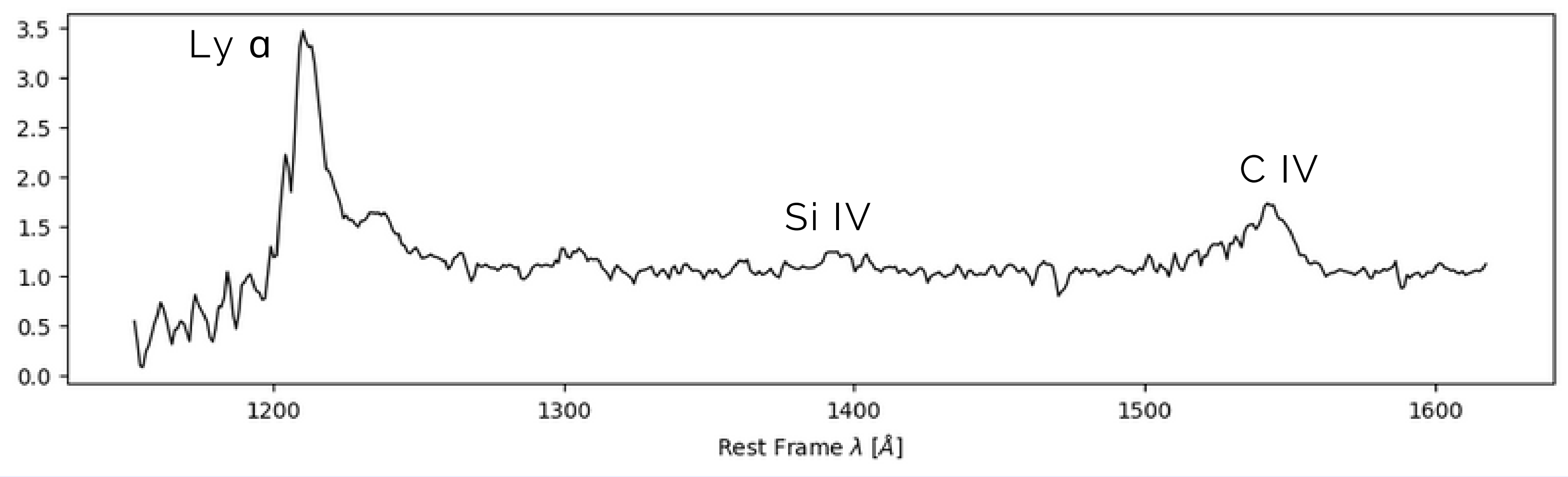

C IVλ1549

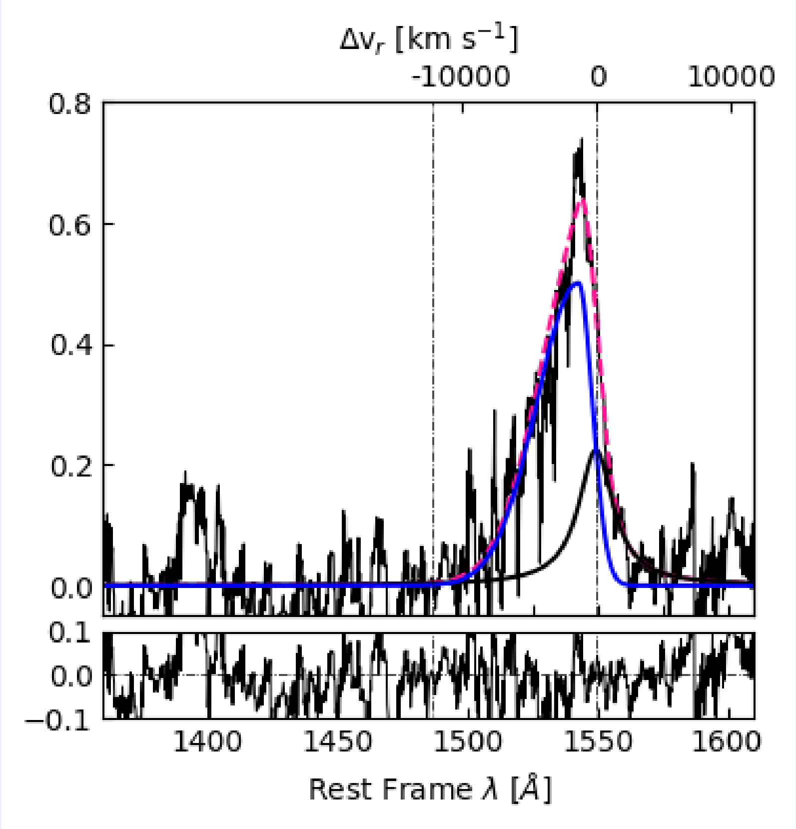

Si IVλ1397+O IV]λ1402

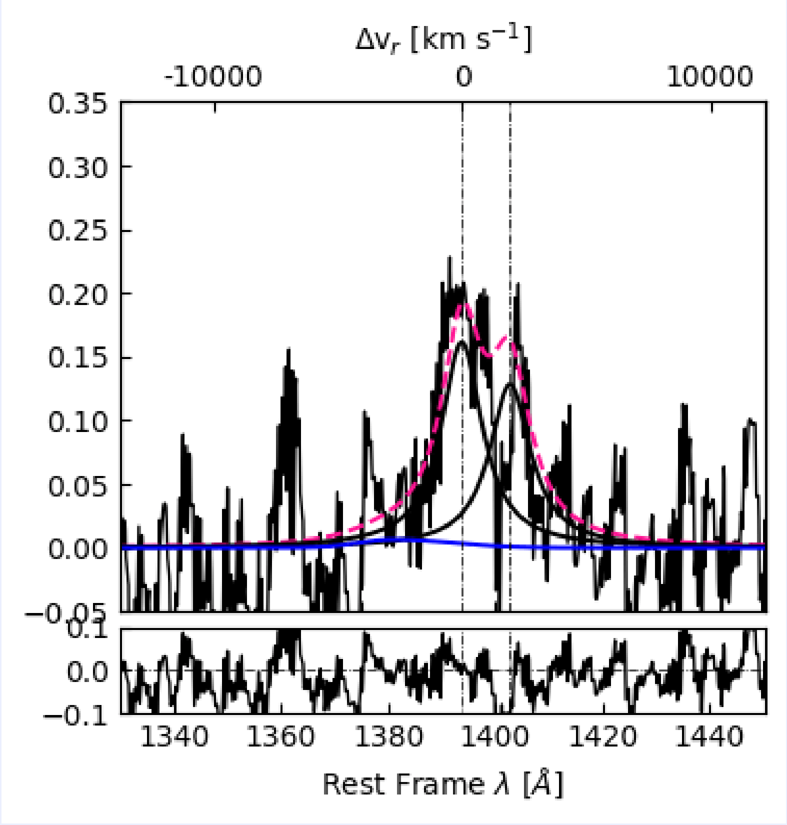

C IVλ1549+He IIλ1640

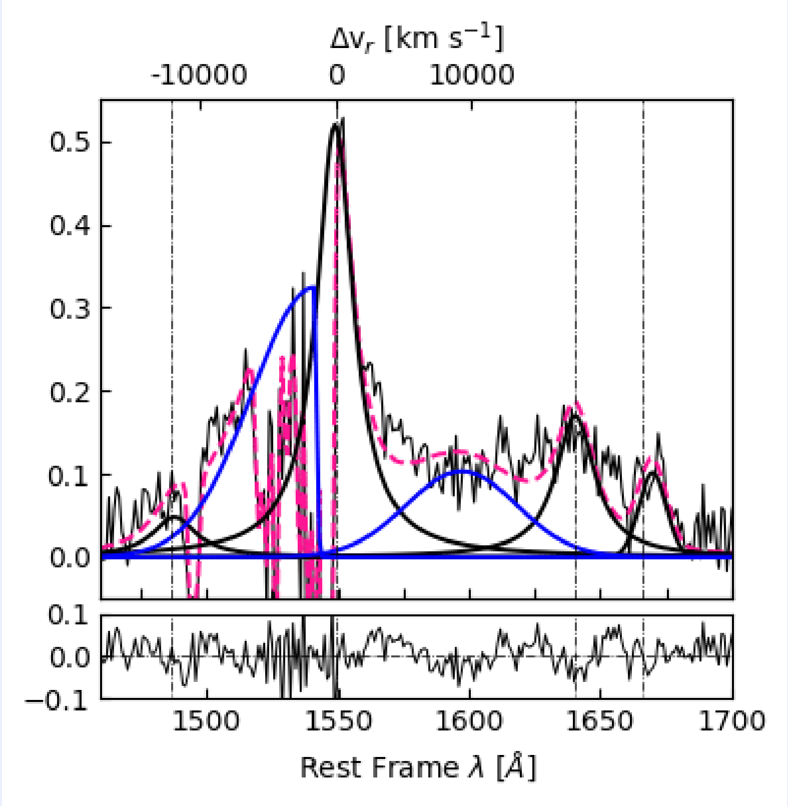

Si IVλ1397+O IV]λ1402

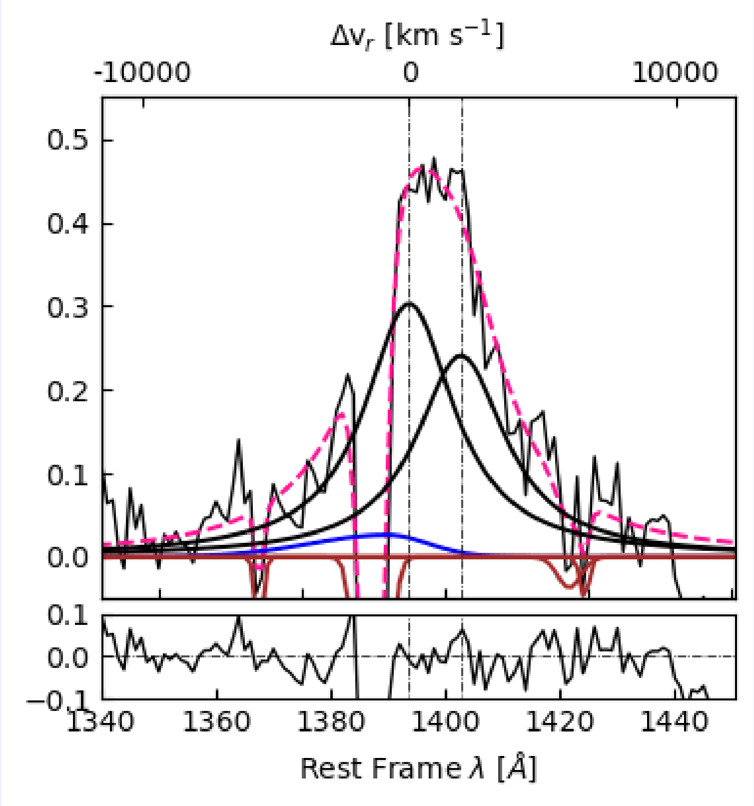

ANALYSIS - **PKS2000-330** & **Q1410+096**

Property	Q1410+096	PKS2000-330
	Optical	
FWHM(Hβ_{full})	3394	3138
c(1/2,Hβ_{full})	54	28
FWHM(Hβ_{BC})	3394	3138
FWHM(Hβ_{NC})	-	1082
FWHM([O III]$_{full}$)	3363	1314
c(1/2,[O III]$_{full}$)	-1404	-425
FWHM([O III]$_{BLUE}$)	5573	1500
FWHM([O III]$_{NC}$)	1379	1082
	UV	
FWHM(Si IV$_{BC}$)	4053	1680
FWHM(Si IV$_{BLUE}$)	6816	3039*
FWHM(C IV$_{full}$)	6311	4950
c(1/2, C IV$_{full}$)	-1746	-1923
FWHM(C IV$_{BC}$)	3293	3141
FWHM(C IV$_{BLUE}$)	10882	7339
FWHM(He II$_{BC}$)	3293	-
FWHM(He II$_{BLUE}$)	9368	-
FWHM(Al III$_{BC}$)	2605	-
FWHM(Si III]$_{BC}$)	2605	-
FWHM(C III]$_{BC}$)	2605	-

1900Å blend

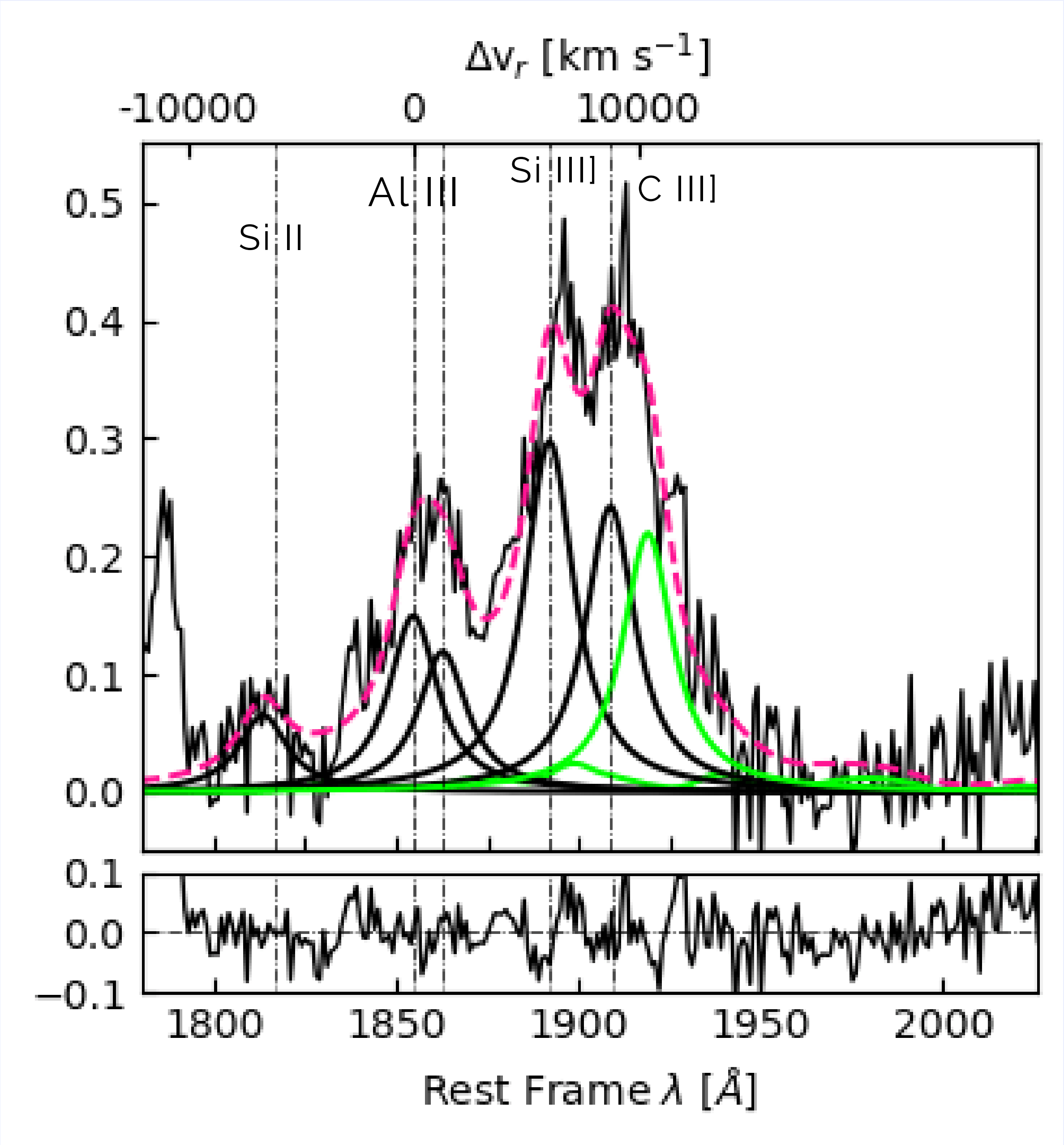

ANALYSIS - **PKS2000-330** & **Q1410+096**

(z = 3.7899) (z = 3.3240)

Property	Q1410+096	PKS2000-330
Optical		
FWHM(Hβ_{full})	3394	3138
c(1/2,Hβ_{full})	54	28
FWHM(Hβ_{BC})	3394	3138
FWHM(Hβ_{NC})	-	1082
FWHM([O III]$_{full}$)	3363	1314
c(1/2,[O III]$_{full}$)	-1404	-425
FWHM([O III]$_{BLUE}$)	5573	1500
FWHM([O III]$_{NC}$)	1379	1082
UV		
FWHM(Si IV$_{BC}$)	4053	1680
FWHM(Si IV$_{BLUE}$)	6816	3039*
FWHM(C IV$_{full}$)	6311	4950
c(1/2, C IV$_{full}$)	-1746	-1923
FWHM(C IV$_{BC}$)	3293	3141
FWHM(C IV$_{BLUE}$)	10882	7339
FWHM(He II$_{BC}$)	3293	-
FWHM(He II$_{BLUE}$)	9368	-
FWHM(Al III$_{BC}$)	2605	-
FWHM(Si III]$_{BC}$)	2605	-
FWHM(C III]$_{BC}$)	2605	-

$$\log M_{\rm BH}({\rm H}\beta) = \log\left\{\left[\frac{\rm FWHM(H\beta)}{1000\ {\rm km\ s^{-1}}}\right]^2\left[\frac{\lambda L_\lambda(5100\text{Å})}{10^{44}\ {\rm erg\ s^{-1}}}\right]^{0.50}\right\} + (6.91 \pm 0.02).$$

Vestergaard & Peterson, 2006

	$\log(M_{\rm H\beta}/M_\odot)$
PKS2000-330	9.21
Q1410+096	9.28

$$\log M_{\rm BH}({\rm C\,IV}) \approx 0.63\log\left[\frac{\lambda L_\lambda(1450\text{Å})}{10^{44}\ {\rm km\ s^{-1}}}\right] + 2\log(\xi_{\rm C\,IV}{\rm FWHM(C\,IV)}) + 0.525,$$

Marziani et al., 2019

$$\log M_{\rm BH,1}\ {\rm AlIII} \approx (0.580^{+0.035}_{-0.040})\log L_{1700,44} + 2\log({\rm FWHM(AlIII)}) + (0.51^{+0.05}_{-0.05}),$$

Marziani et al., 2021 (subm.)

ANALYSIS - **PKS2000-330** & **Q1410+096**

Property	Q1410+096	PKS2000-330
	Optical	
FWHM(Hβ_{full})	3394	3138
c(1/2,Hβ_{full})	54	28
FWHM(Hβ_{BC})	3394	3138
FWHM(Hβ_{NC})	-	1082
FWHM([O III]$_{full}$)	3363	1314
c(1/2,[O III]$_{full}$)	-1404	-425
FWHM([O III]$_{BLUE}$)	5573	1500
FWHM([O III]$_{NC}$)	1379	1082
	UV	
FWHM(Si IV$_{BC}$)	4053	1680
FWHM(Si IV$_{BLUE}$)	6816	3039*
FWHM(C IV$_{full}$)	6311	4950
c(1/2, C IV$_{full}$)	-1746	-1923
FWHM(C IV$_{BC}$)	3293	3141
FWHM(C IV$_{BLUE}$)	10882	7339
FWHM(He II$_{BC}$)	3293	-
FWHM(He II$_{BLUE}$)	9368	-
FWHM(Al III$_{BC}$)	2605	-
FWHM(Si III]$_{BC}$)	2605	-
FWHM(C III]$_{BC}$)	2605	-

Property	Q1410+096	PKS2000-330
	Optical	
I(Hβ_{BC})	1.0	0.93
Shift(Hβ_{BC})	54	28
I(Hβ_{NC})	-	0.072
Shift(Hβ_{NC})	-	-46
I([O III]$_{BLUE}$)	0.73	0.42
Shift([O III]$_{BLUE}$)	-1255	-827
I([O III]$_{NC}$)	0.27	0.58
Shift([O III]$_{NC}$)	-260	-263
	UV	
I(C IV$_{BC}$)	0.58	0.29
Shift(C IV$_{BC}$)	0	81
I(C IV$_{BLUE}$)	0.42	0.71
Shift(C IV$_{BLUE}$)	-1525	-1219
I(Al III$_{BC}$)	1.0	-
Shift(A III$_{BC}$)	0	-

CONCLUSIONS

- PKS2000-330 and Q1410+096 are very similar in the optical context. However, there is a clear difference seen in the UV;
- The difference may be a dynamic effect from the jet in the radio-loud source (PKS2000-330);
- The UV region of the radio-quiet (Q1410+096) suggests high metallicity, which can be related with a difference in the chemical evolution in both quasars.

Thank you!
Obrigada!

adeconto@iaa.es